

Search for Low Mass Exotic Baryons in One Pion Electroproduction Data Measured at JLAB

B. Tatischeff*

¹*Institut de Physique Nucléaire*

CNRS/IN2P3, F-91406 Orsay Cedex, France

²*Univ Paris-Sud, Orsay, F-91405*

E. Tomasi-Gustafsson†

DAPNIA/SPhN, CEA/Saclay, 91191 Gif-sur-Yvette Cedex, France

(Dated: March 10, 2017)

Abstract

This paper aims to give further evidence for the existence of low mass exotic baryons. Narrow structures in baryonic missing mass or baryonic invariant mass were previously observed during the last ten years. Since their existence is sometimes questionable, the structure functions of one pion electroproduction cross sections, measured at JLAB, are studied to add informations on the possible existence of these narrow exotic baryonic resonances.

PACS numbers: 25.30.Dh, 14.20.Gk, 13.60.Rj, 13.40.-f

*e-mail : tati@ipno.in2p3.fr

†e-mail : etomasi@cea.fr

I. INTRODUCTION

This paper is dedicated to a reanalysis of existing data on one pion electroproduction cross sections measured at JLAB. Although observed in several reactions and in different kinematical conditions, the narrow low mass baryonic structures are sometimes considered with skepticism. Indeed a few dedicated experiments were not able to observe them. This result will be discussed below. In order to disentangle that situation, it is necessary to study new data obtained with a fairly good resolution. The one pion electroproduction cross sections, measured at JLAB, are, in principle, appropriate for such study. This study is significant since these structures - if any - will be exotic. Several reasons plead in favor of their exoticism:

- their widths, typically of the order of $\text{FWHM} \approx 10$ to 20 MeV are much smaller than the widths of PDG (Particle Data Group) N^* or Δ resonances,
- the first resonances have a mass lower than the pion production threshold mass,
- there is no room for these resonances, in the mass range discussed here, within the many-quark models for baryons if we consider only qqq configurations [1].

In the second section, the results for narrow low mass baryonic structures, mainly observed in SPES3 (Saturne), are recalled. Their masses are compared to a careful scrutiny of many different data, obtained by different collaborations, for different physical studies, with hadronic as well as leptonic probes. The cross sections of the structure functions, from backward π^0 electroproduction on protons, measured by the Hall A Collaboration [2] are considered in sections III.A. Data on the structure functions from the $ep \rightarrow e'n\pi^+$ reaction, measured by the CLAS Collaboration [3] in Hall B, are discussed in section III.B. The results of the present analysis are discussed in section IV, and the paper is concluded in section V.

As mentioned above, narrow structures were observed more often in experiments using incident hadrons than with incident leptons. In the spectra of the reaction $ep \rightarrow e'\pi^+X^0$ studied [4] at JLAB (Hall A), no significant signal was observed in the range $0.97 \leq M_{X^0} \leq 1.06$ GeV. In a high-resolution experiment studied at MAMI [5], no narrow nucleon resonance below pion threshold was observed in the $H(e,e'\pi^+)X$ or $D(e,e'p)X$ reactions. No low-lying exotic baryons (at masses $M=1004$ and 1044 MeV) were observed at TRIUMF [6] in a double radiative pionic capture on hydrogen. These three dedicated experiments looked at narrow baryonic structures with masses below the pion production mass. The absence of signal

in these experiments using incident leptons, can be related to the fact that these narrow structures may have a small coupling to nucleon, their excitation being favored for reactions involving two baryons (for example excitation through intermediate dibaryons).

The lack of observation of narrow baryonic structures below pion production mass, constitutes a further reason to look at data obtained with incident leptons, concerning the mass range above pion production threshold.

II. RECALL OF ALREADY PUBLISHED DATA SHOWING THE EXISTENCE OF NARROW LOW MASS BARYONS

Previous experiments, performed at SPES3 (Saturne), thanks to good resolution and high statistics, exhibit narrow structures in different hadronic masses. Only results concerning baryons will be discussed here. Two reactions:

$$p + p \rightarrow p + p + X \quad (1)$$

and

$$p + p \rightarrow p + \pi^+ + X \quad (2)$$

were studied. Structures were observed in the missing mass M_X of reaction (2) [7] and in the invariant mass M_{pX} of reaction (1) and in the invariant masses $M_{p\pi^+}$ and M_{π^+X} of reaction (2) [8]. The observation in different conditions (reaction, incident energy, spectrometer angle, or observable) at the same mass (within ± 3 MeV) was considered a confirmation of their existence. This is summarized in Fig. 1 of Ref. [8] in the mass range $1.0 \leq M \leq 1.4$ GeV. In the figure, columns (a) to (f) correspond to different variables or incident energies of reaction (2), columns (g) and (h) correspond to reaction $dp \rightarrow ppX$ at two different incident energies [8], column (i) describes data from $\gamma n \rightarrow p\pi^- \pi^0$ reaction studied at MAMI [9] and column (j) to data from $\gamma p \rightarrow \pi^+ n$ reaction studied at Bonn [10]. The narrow structures masses observed are: 1004, 1044, 1094, 1136, 1173, 1249, 1273, 1339, and 1384 MeV.

Additional signatures of narrow baryonic structures, were observed either in dedicated experiments or extracted from cross sections obtained and published by different authors studying other problems. They are quoted in [7] and [8] and will not be recalled here.

Precise spectra of the $p(\alpha, \alpha')X$ reaction were obtained at SPES4 (Saturne) in order to study the radial excitation of the nucleon in the $P_{11}(1440$ MeV) Roper resonance. The

measurements were done using a $T_\alpha=4.2$ GeV incident beam. The spectrum at $\theta_{\alpha'}=0.8^\circ$ was published in [11] and the spectrum at $\theta_{\alpha'}=2^\circ$ was published in [12]. A first large peak around $M_X \approx 1130$ MeV ($\omega \approx 240$ MeV), was associated to the projectile excitation, and a second large peak around $M_X \approx 1345$ MeV ($\omega \approx 510$ MeV), was associated to the target excitation. Above them lie narrow peaks [13], characterized by a large number of standard deviations, since the highest channel at $\theta=0.8^\circ$ contains approximately 2.5×10^4 events (see Fig. 2 and 3). These structures were not discussed by the authors. A detailed discussion of the spectrometer and of the detection performances was given in [13] and will not be repeated here as well as the checks performed and the final precision obtained. Figs. 2 and 3 show the spectra. Table 1 gives the correspondance among the letters naming the structures, their masses and the masses of the corresponding structures extracted from SPES3 data. Such correspondance is illustrated in Fig. 4.

Finally we list, in the mass range studied here: $1.1 \leq M \leq 1.56$ GeV, eight narrow masses at $M=1136, 1173, 1249, 1273, 1339, 1384, 1480,$ and 1540 MeV. A well separated structure at $M=1479$ MeV was extracted from $pp \rightarrow ppX$ and $pp \rightarrow pp\pi^0$ reactions [8]. Several other structures were extracted in the same work, at larger masses, but with a too small separation to be seen in the two lower resolution experiments of one pion electroproduction on proton, considered in the present work.

III. ANALYSIS OF ONE PION ELECTROPRODUCTION STRUCTURE FUNCTION CROSS SECTIONS MEASURED AT JLAB

The reactions $\gamma^* + p \rightarrow \pi^0 + p$ and $\gamma^* + p \rightarrow \pi^+ + n$ have been measured at different kinematical conditions.

The differential cross sections are expressed by the following equation [14]:

$$d^2\sigma/d\Omega_p = d^2\sigma_T/d\Omega_p + \varepsilon d^2\sigma_L/d\Omega_p + \sqrt{[2\varepsilon(1 + \epsilon)]} d^2\sigma_{LT}/d\Omega_p \cos(\Phi) + \varepsilon d^2\sigma_{TT}/d\Omega_p \cos(2\Phi). \quad (3)$$

The σ_T , σ_L , σ_{TL} , and σ_{TT} structure functions are bilinear combinations of the helicity amplitudes, depending only on the variables Q^2 , W , and θ . $d^2\sigma_T$ is the transverse part of the cross section, $d^2\sigma_L$ is the longitudinal part of the cross section, and $d^2\sigma_{TL}$ and $d^2\sigma_{TT}$ are interference parts.

θ is the polar angle between initial and final protons, in the CM system defined by the final proton and missing particle ($\bar{q} + \bar{p}$). $\varepsilon=[1+2(1+\nu^2/Q^2)\tan^2\theta_e/2]^{-1}$ is the polarization parameter or the virtual photon polarization. $\nu=E_i - E_f$ is the energy transfer. $Q^2=4 E_i E_f \sin^2\theta_e/2=(\bar{k}_e - \bar{k}'_e)^2$ is the four momentum transfer squared. M is the proton mass and $W=[M^2 + 2M\nu - Q^2]^{1/2}$ is the mass of the hadronic system. The structure functions are plotted versus W . Φ is the azimuthal angle between the leptonic and the hadronic planes.

The structure functions σ_{TT} , σ_{TL} , and the linear combination $\sigma_T + \varepsilon\sigma_L$ were obtained by fitting the Φ dependence of the cross section to a function of the form:

$$F(\theta) = A + B \cos(\Phi) + C \cos(2\Phi). \quad (4)$$

They are described theoretically by the phenomenological MAID model [15]. The MAID model uses an effective Lagrangian approach to calculate the Born background, including ω and ρ meson calculations. The background is unitarized in the K-matrix approximation. The resonant amplitudes are determined by fitting the world pion production data. The MAID2003 model is a fit to predominantly $\pi^0 p$ channel.

The MAID calculations describe the main shapes of the structure functions, especially at small θ angles.

We compute MAID using all baryonic resonances from $P_{33}(1232)$ up to $F_{37}(1950)$ [15], although the last ones lie outside the range of study. The calculation holds background, resonances and interferences between both.

MAID contains the experimental phase shifts and includes most of the known physics, in electroproduction processes. Therefore, in order to enhance the physics which is not contained in MAID, we build the difference between the experimental spectra and the MAID results. The figures show that such difference exhibits narrow structures located at similar masses. Then, we fit the results of the subtraction of data from MAID. Interferences between these small eventual structures, and the background and broad resonances exist. Since the amplitudes of broad PDG resonances (and Born background) vary little in the smaller range of each narrow resonance, the extracted position of these narrow resonances should be not much affected by these interference terms. Such effect exist in all experiments since these resonances lie always above other physics and background. However it was observed, see

Fig. 1, that the masses observed were quite stable.

The fits shown are obtained using gaussians and masses given in previous section, namely those extracted from previous experiments. No attempt is done to adjust any mass. The width also is taken, arbitrarily, to be $\sigma=24$ MeV, in both reactions, without any attempt to adjust it. The experimental statistical errors are kept as errors for the data minus MAID values. In some cases, the large error bars prevent to give firm confidence on the peak extractions which were only done in view of consistency.

In these experiments, the masses below pion production cannot be observed. Also the structure at $M=1094$ MeV is missing since the data start at $M=1110$ MeV.

When σ_{TT} and σ_{TL} structure functions are interference terms, with possible positive and negative values, the third structure function: $\sigma_T + \epsilon \sigma_L$ is positive, since obtained by the square of amplitudes. This is the case for data and for MAID results. However the difference between both involve interference terms between "classical amplitudes", described by MAID, and new amplitudes from narrow baryons which existence is discussed. Therefore, after the difference, the result of this structure function $\sigma_T + \epsilon \sigma_L$ can be negative. We suppose that the amplitudes of the Born background and broad resonances vary slowly in the range of narrow resonances. This justifies, as already pointed out, the statement that our procedure should exhibit narrow peaks, if any, close to their genuine masses.

A. The $\gamma^*p \rightarrow \pi^0 p$ reaction

The backward cross sections of the structure functions of the $\gamma^*p \rightarrow \pi^0 p$ reaction were measured by the Hall A Collaboration [2] at four angles θ and at $Q^2=1$ GeV².

1. The $\sigma_T + \epsilon \sigma_L$ structure function

Fig. 5 shows the $\sigma_T + \epsilon \sigma_L$ structure function at $\theta=167.16^\circ$ in inserts (a) and (b) and at $\theta=157.67^\circ$ in inserts (c) and (d). Inserts (a) and (c) show the data (full circles) the MAID results (dashed curves) and the difference (full stars). Inserts (b) and (d) show the previous difference (full circles), the peaks for individual masses and the total spectrum obtained with assumption of no interference. At both angles a large peak is observed at a somewhat larger mass ($M \approx 1200$ MeV instead $M=1173$ MeV). A narrow structure at $M \approx 1540$ MeV is

well defined in insert (b). Fig. 6 shows the corresponding results for $\theta=155.05^\circ$ in inserts (a) and (b) and at $\theta=145.59^\circ$ in inserts (c) and (d). We observe that the quality of the fit with MAID, at backward angles, gets spoiled when the angles decrease.

Fig. 7 shows the angular variation versus θ of the yield of the seven narrow masses as extracted from Figs. 5 and 6. The error bars here are arbitrarily put to 20% of the height of each peak, increased by 10% of the highest peak in order to get a reasonable error for small peaks. We observe a smooth and continuous variation of the observed yields. The curves are a tentative fit of the points by the function

$$F = \sum_{i=0}^2 a_i \cos^{2i} \theta. \quad (5)$$

In the small angular range covered by the experiment, all seven peaks show a similar behavior. We do not attempt to draw conclusions on the spin and parity of the narrow resonances from the present, restricted angular distributions.

2. The σ_{TT} structure function

Fig. 8 shows the results for the σ_{TT} structure function at $\theta=167.16^\circ$ in inserts (a) and (b), and at $\theta=157.67^\circ$ in inserts (c) and (d). Here also the data, the MAID results, the difference between both, and the fits of the peaks are defined as previously for the $\sigma_T + \epsilon\sigma_L$ structure function. Fig. 9 shows the results for the σ_{TT} structure function at $\theta=151.05^\circ$ in inserts (a) and (b), and at $\theta=145.59^\circ$ in inserts (c) and (d). Fig. 10 shows the angular variation of the seven σ_{TT} structure functions corresponding to the seven peaks studied. In all inserts the yield for the largest angle is close to zero. A rather good continuity is observed, except in insert (a) which corresponds to $M=1136$ MeV narrow structure peak. The same function as previously, Eq (5), is used for the fits.

3. The σ_{TL} structure function

Fig. 11 shows the results for the σ_{TL} structure function at $\theta=167.16^\circ$ in inserts (a) and (b), and at $\theta=157.67^\circ$ in inserts (c) and (d). Fig. 12 shows the results for the σ_{TL} structure function at $\theta=151.05^\circ$ in inserts (a) and (b), and at $\theta=145.59^\circ$ in inserts (c) and (d). In this structure function, the fit with MAID is poor at all angles; at the smallest angle $\theta=145.59^\circ$,

the peak at $M=1210$ MeV reaches only 25% of its experimental value. Fig. 13 shows the angular variation of the seven σ_{TL} structure functions, corresponding to the seven peaks studied. We observe the continuous behavior of the other distributions, again fitted with the same function versus $\cos\theta$. Here again, the small angular range prevents to give strong importance to these fits which are merely an indication of similar shapes between all peaks.

B. The $\gamma^*p \rightarrow \pi^+n$ reaction

The $ep \rightarrow e'n\pi^+$ reaction was measured at JLAB in Hall B, by the CLAS Collaboration [3]. These data are less precise than those discussed above from Hall A. The cross sections of the three structure functions were extracted at four values of four momentum transfers: $Q^2=0.3, 0.4, 0.5,$ and 0.6 GeV², and at ten angles $\theta=7.5^0, 22.5^0, 37.5^0, 52.5^0, 67.5^0, 82.5^0, 97.5^0, 112.5^0, 127.5^0,$ and 142.5^0 . We analyze here the difference between data and MAID calculations for two Q^2 values $Q^2=0.3$ and 0.4 GeV², and six center of mass angles $\theta=7.5^0, 22.5^0, 52.5^0, 67.5^0, 97.5^0,$ and 127.5^0 . The data at $\theta=142.5^0$ are very imprecise. No data are available at $Q^2=0.6$ GeV² for the hadronic system mass W larger than $W=1.4$ GeV. As previously discussed, the figures illustrate the experimental structure functions, the MAID results and their differences on the left side, whereas, on the right side these differences are plotted with the corresponding fits.

1. The $\sigma_T + \epsilon\sigma_L$ structure functions

Fig. 14 exhibits the $\sigma_T + \epsilon\sigma_L$ structure functions at $\theta=7.5^0$ and $Q^2=0.3$ GeV² in inserts (a) and (b), and at $\theta=7.5^0$ and $Q^2=0.4$ GeV² in inserts (c) and (d). For this structure function, and at such small angle, MAID describes fairly well the data up to $W=1350$ MeV, however a difference remains which can be fitted reasonably well with the same masses as before. The next figures Fig. 15, Fig. 16, Fig. 17, Fig. 18, and Fig. 19, correspond respectively to the same analysis but different angles $\theta=22.5^0, 52.5^0, 67.5^0, 97.5^0,$ and 127.5^0 . Some masses, i.e. at $M=1173$ MeV, 1210 MeV and 1480 MeV are better defined than the others. Here again the cross sections at $Q^2=0.3$ GeV² and $Q^2=0.4$ GeV² are not very different. Fig. 20 shows the angular variations of the seven $\sigma_T + \epsilon\sigma_L$ structure functions, corresponding to the seven narrow structure masses studied. The error bars are again defined as explained above for

the first reaction. Full circles correspond to $Q^2=0.3 \text{ GeV}^2$ and empty circles correspond to $Q^2=0.4 \text{ GeV}^2$. The data corresponding to both four-momentum transfers are close, most of the time. Full curves correspond to tentative fits with the function defined above, Eq. 5; in one case, insert (a), the fit is obtained with an odd function of θ , namely $\sin 2\theta$.

2. The σ_{TT} structure functions

Fig. 21 shows the results for σ_{TT} structure function at $\theta=7.5^\circ$, in inserts (a) and (b) for $Q^2=0.3 \text{ GeV}^2$ and in inserts (c) and (d) for $Q^2=0.4 \text{ GeV}^2$ data. At this angle, there is no precise experimental data in the mass range $1230 \leq M \leq 1340 \text{ MeV}$. The description by MAID fails totally to describe the data. The results for $\theta=22.5^\circ$ are shown in Fig. 22, inserts (c) and (d) for $Q^2=0.3 \text{ GeV}^2$ and in Fig. 23, inserts (c) and (d) for $Q^2=0.4 \text{ GeV}^2$ data. Fig. 24 show the results of the σ_{TT} structure function at $Q^2=0.3 \text{ GeV}^2$. Inserts (a) and (b) show the results obtained at $\theta=52.5^\circ$, and inserts (c) and (d) show the results at $\theta=67.5^\circ$. Fig. 25 shows the results identical to those from Fig. 24, but for $Q^2=0.4 \text{ GeV}^2$. Fig. 26 shows the results for σ_{TT} structure function at $\theta=97.5^\circ$ at $Q^2=0.3 \text{ GeV}^2$ in inserts (a) and (b) and at $Q^2=0.4 \text{ GeV}^2$ in inserts (c) and (d). The error bars decrease with increasing angles, and consequently the structure's definitions are good. Fig. 27 shows the σ_{TT} structure function at $\theta=127.5^\circ$ at $Q^2=0.3 \text{ GeV}^2$ in inserts (a) and (b) and at $Q^2=0.4 \text{ GeV}^2$ in inserts (c) and (d).

Fig. 28 shows the angular variation of the σ_{TT} structure function with an attempt to fit the data with a low order polynomial of $\cos^{2n} \theta$. The full circles correspond to $Q^2=0.3 \text{ GeV}^2$, and the empty circles correspond to $Q^2=0.4 \text{ GeV}^2$. We observe that in several inserts, corresponding to different narrow mass structures, the fitted curves describe very satisfactorily most of the data.

3. The σ_{TL} structure functions

Fig. 29 shows the cross-section of the σ_{TL} structure function at $\theta=7.5^\circ$. Inserts (a) and (b) correspond to $Q^2=0.3 \text{ GeV}^2$, inserts (c) and (d) correspond to $Q^2=0.4 \text{ GeV}^2$. Here also, as it was the case at the same angle for the σ_{TT} structure function, there is no precise experimental data in the mass range around $M \approx 1300 \text{ MeV}$. The results at 22.5° are

shown in Fig. 22 inserts (a) and (b) for $Q^2=0.3 \text{ GeV}^2$, and in Fig. 23 inserts (a) and (b) for $Q^2=0.4 \text{ GeV}^2$. Fig. 30 shows the results for $Q^2=0.3 \text{ GeV}^2$ $\theta=52.5^\circ$ in inserts (a) and (b), and $\theta=67.5^\circ$ in inserts (c) and (d). The peak's extraction from insert (b) is meaningless, it is only shown for sake of consistency. Fig. 31 shows the results corresponding to the same angles but for $Q^2=0.4 \text{ GeV}^2$. Here again the $\theta=52.5^\circ$ data do not allow to extract peaks. Fig. 32 shows the results for $\theta=97.5^\circ$ $Q^2=0.3 \text{ GeV}^2$ in inserts (a) and (b), and $Q^2=0.4 \text{ GeV}^2$ in inserts (c) and (d). Fig. 33 shows the results for $\theta=127.5^\circ$ $Q^2=0.3 \text{ GeV}^2$ in inserts (a) and (b), and $Q^2=0.4 \text{ GeV}^2$ in inserts (c) and (d).

Fig. 34 shows the angular variations of the σ_{TL} structure function. The insert (a) ($M=1136 \text{ MeV}$) is fitted with an odd function, $1.6 \sin 2\theta$; the insert (b) ($M=1210 \text{ MeV}$) is fitted with the function $4.5 \cos \theta$. The other curves are fits to the points with a low order polynomial of $\cos^{2n} \theta$.

IV. DISCUSSION

Whereas clear peaks are observed in both sides of the mass range studied here, this is not always the case in the mass range $M \approx 1.4 \text{ GeV}$. No attempt to get a better adjustment by shifting the masses, is done on the fits shown above. Most of the extracted structure function surfaces, exhibit a smooth angular variation. This result justifies, *a posteriori*, the attempt to associate the difference between structure functions and MAID, with the existence of narrow baryonic structures.

One argument not to attribute the differences described above to deficiencies in MAID, lies in the smallness of the widths of the residual peaks. Indeed, we expect that an eventually poor description of the data by MAID would result in broader effects.

A. Possible isospin values for the narrow structures

Both reactions were studied at complementary angles, roughly in the range $0 \leq \theta \leq 140^\circ$ for the $\gamma^*p \rightarrow \pi^+n$ reaction and $140 \leq \theta \leq 170^\circ$ for the $\gamma^*p \rightarrow \pi^0p$ reaction. However in both reaction, the four momentum transfer is different. We observe small variations of the cross section between $Q^2=0.3 \text{ GeV}^2$ and $Q^2=0.4 \text{ GeV}^2$, but an extrapolation up to $Q^2=1 \text{ GeV}^2$ may not be justified. Both reactions are related by isospin Clebsh-Gordan coefficients. If we

neglect the variation of the structure function due to different Q^2 values, the intermediate resonance N^* with isospin 1/2, will favor π^+n by a factor of two, and the intermediate resonance Δ with isospin 3/2 will favor π^0p by a factor of two. Figs. 20, 28, and 34 show the angular variations of the structure functions, respectively $\sigma_T + \epsilon\sigma_L$, σ_{TT} , and σ_{TL} , with the results of both reactions. The results from the $ep \rightarrow ep'\pi^0$ reaction at backward angles are drawn with stars. Both reactions display cross sections with smooth behavior for several inserts. A continuous curve reproducing the behavior for both reactions, may be considered as an indication of the excitation of isospin 3/2 resonance. In this case, the increase by a factor of two, due to isospin, could be compensated by a reduction by a similar factor due to the increase in Q^2 from 0.3-0.4 GeV² up to 1 GeV².

In order to tentatively suggest isospins for the narrow structures, we apply the following rule: when the structure function of the $\gamma^*p \rightarrow \pi^0p$ reaction and the structure function of the $\gamma^*p \rightarrow \pi^+n$ reaction follow the same line, we propose an isospin value of 3/2 for the baryonic structure; when the structure function of the first reaction is much smaller than the one of the second reaction, we suggest an isospin 1/2. Table 2 shows the possible isospin attributions. We observe that the structures at $W=1136$ MeV (insert (a)), should have isospin $T=1/2$, since all three structure functions predict such value. Isospin $T=3/2$ is predicted twice for $M=1210$ MeV, $M=1277$ MeV, and $M=1480$ MeV. Isospin $T=1/2$ is predicted twice for $M=1339$ MeV, $M=1384$ MeV, and $M=1540$ MeV. Therefore narrow structures at $M=1210$ MeV and $M=1277$ MeV could be "substructures" of the broad PDG $\Delta(1232)$ P_{33} resonance; just as the narrow structure at $M=1480$ MeV could be a "substructure" of the broad PDG $\Delta(1600)$ P_{33} resonance which total width is estimated [16] to be as large as 350 MeV. The narrow structures at $M=1339$ MeV, $M=1384$ MeV, and $M=1540$ MeV could be parts of the $N^*(1440)$ P_{11} which total width is also estimated [16] to be as large as 350 MeV, and (or) part of the $N^*(1520)$ D_{13} broad PDG baryonic resonance.

B. Possible spin values for the narrow structures

The curves which fit the angular distributions drawn in Figs. 20, 28, and 34 are obtained, besides a few exceptions, using low order polynomials of $x = \cos^2 \theta$. Due to the relative imprecision of the data, and their rather reduced number, the fits presented are not conclusive. It is not possible to identify the angular distributions with theoretical angular distributions

[17] [18] which are given for cross-sections and not for structure functions. Moreover the theoretical angular distributions may be more complicated for increasing J values of the narrow baryonic resonances spins. Indeed these angular distributions are polynomials of $\cos^2 \theta$, of the order $2J-1$.

The angular distributions of the $\sigma_T + \epsilon\sigma_L$ structure function differ from one narrow structure mass to another. Since the data of the $M=1277$ MeV structure (insert (c)) scatter too much, the fitted curve may be meaningless. The experimental distributions of the other inserts are continuous.

The angular distributions of the σ_{TT} structure function show a smooth behavior for the inserts (a), (b), (c), (e), and (g).

We observe that the distributions of the σ_{TL} structure functions have the same shape for the masses corresponding to inserts (c), (d), (e), and (f), namely that they all are proportional to $f = x - x^2$ (where x stands for $\cos^2 \theta$) with different translations. The data are continuous for the inserts (a), (b), (d), (e), and (g).

Concluding this discussion, we observe that no spin attribution can be made, and only the comparison between π^0 and π^+ electroproduction, may eventually allow to suggest isospin values.

V. CONCLUSION

The paper presents a contribution to the study of narrow exotic low mass baryons. Above pion production threshold, several narrow baryonic structures could be extracted from experiments using incident leptons. Several results of this kind were presented in [8] and were not recalled here. The two discussed experiments, namely one pion electroproduction on proton, were performed with another aim; their results were then not obtained with an appropriate resolution.

We have shown that the description of the measurements with MAID was sometimes more qualitative than quantitative. The difference between data and results from MAID calculations, exhibits narrow peaks, better defined in both sides of the studied range. We have shown that the entire range can be described by structures at the masses extracted from previous experiments performed with hadrons and previous analysis. We conclude that these data, although they do not contain by themselves an unambiguous signature,

they nevertheless increase the confidence in the genuine existence of these narrow baryonic structures. The comparison between both electroproduction reactions, allowed us to suggest possible isospins for these narrow baryonic structures.

Thanks are due to H. Fonvieille for her interest and critical remarks.

-
- [1] S.Capstick and W.Roberts, Prog. Part. Nucl. Phys.**45**, 08241 (2000).
 - [2] G. Laveissière *et al.*, The Hall A Collaboration, Phys. Rev. C**69**, 045203 (2004).
 - [3] H. Egiyan *et al.*, Phys. Rev. C**73**, 025204 (2006).
 - [4] X.Jiang *et al.* Phys. Rev. C**67**, 028201 (2003).
 - [5] M.Kohl *et al.*, arXiv:nucl-ex/0304013 (2003).
 - [6] P.A.Zolnierczuk *et al.*, arXiv:nucl-ex/0403046 (2004).
 - [7] B. Tatischeff *et al.*, Phys. Rev. Lett. **79**, 601 (1997).
 - [8] B. Tatischeff *et al.*, Eur. Phys. J. A **17**, 245 (2003); *ibid* Surveys in High Energy Physics, **19**, 55 (2004); *ibid* Phys. Rev. C**72**, 034004 (2005).
 - [9] A. Zabrodin *et al.*, Phys. Rev. C**60**, 055201 (1999).
 - [10] H.W. Dannhausen, E.J. Durwen, H.M. Fisher, M. Leneke, W. Niehaus, and F. Takasaki, Eur. Phys. J. A**11**, 441 (2001).
 - [11] H.P. Morsch *et al.*, Phys. Rev. Lett. **69**, 1336 (1992); H.P. Morsch and P. Zupranski, Phys. Rev. C**61**, 024002 (1999).
 - [12] H.P. Morsch, Proceedings of the Dixieme Journee Thematique de l'IPN d'Orsay (1995).
 - [13] B.Tatischeff, arXiv:nucl-ex/0404042
 - [14] P.A. Guichon, G.Q. Liu and A.W. Thomas, Nucl. Phys. A**551**, 606 (1995).
 - [15] D. Drechsel, S.S. Kamalov, and L. Tiator, Nucl. Phys. A**645**, 145 (1999).
 - [16] Particle Data Group, Phys. Lett. B**592**, 1 (2004).
 - [17] R.F. Peierls, Phys. Rev. **118**, 325 (1960).
 - [18] S. Gasiorowicz, Elementary Particle Physics, John Wiley and Sons, Inc. editors, (1966).

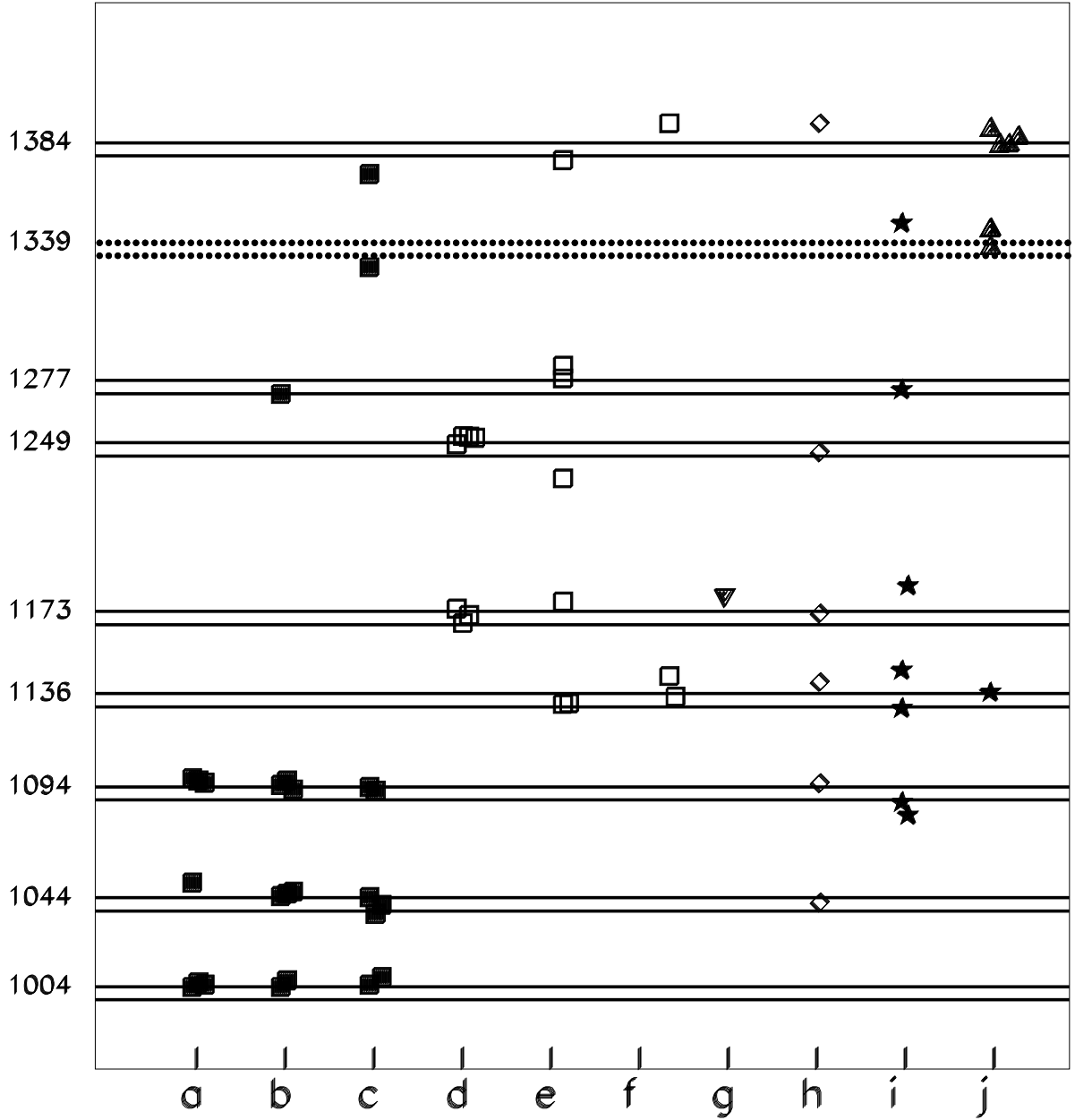


FIG. 1: Narrow-structure baryonic masses observed in cross-sections from different reactions [8].

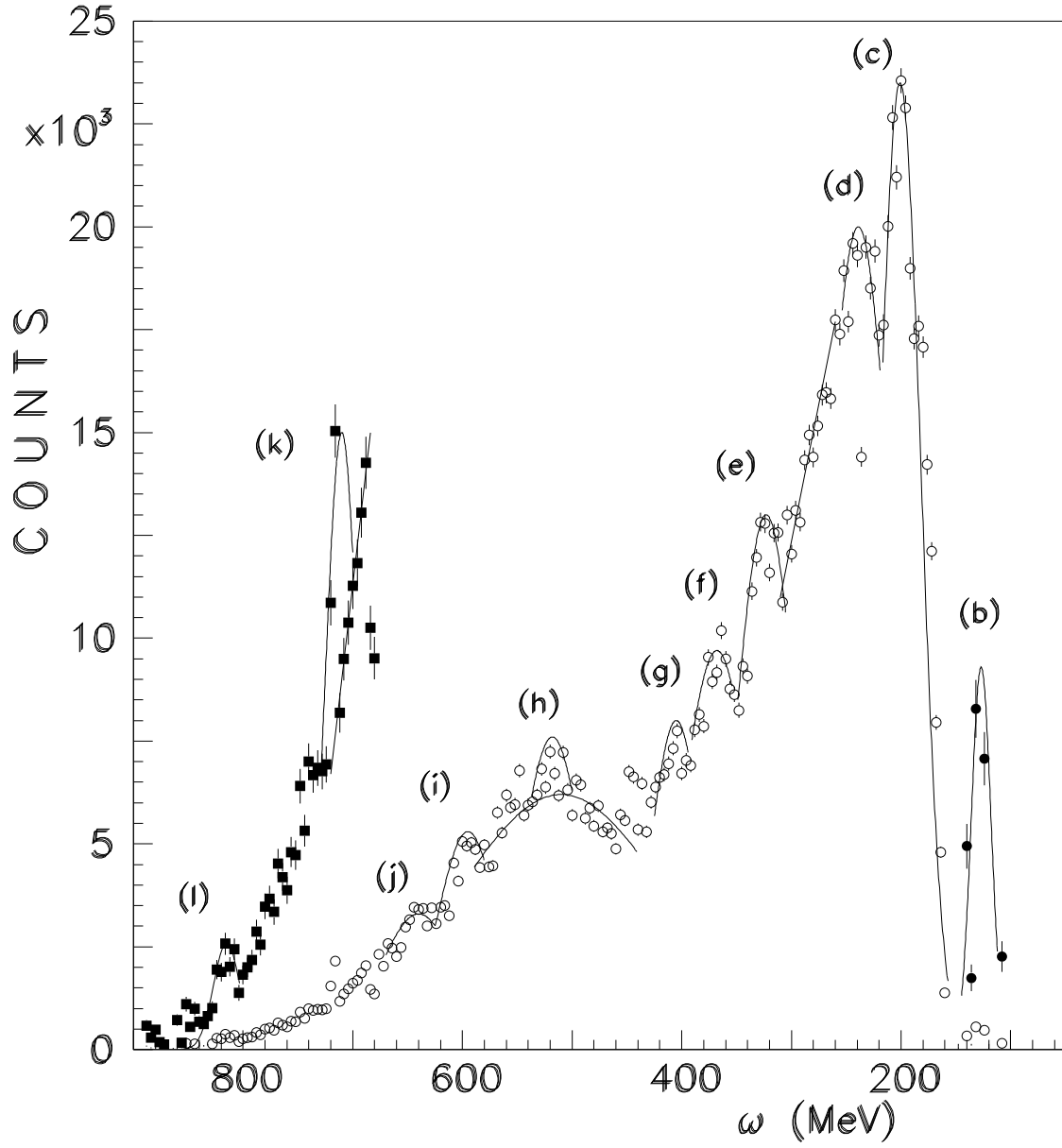


FIG. 2: Spectra of the $p(\alpha, \alpha')X$ reaction studied at SPES4 (Saturne) with $T_\alpha=4.2$ GeV and $\theta=0.8^\circ$ [11].

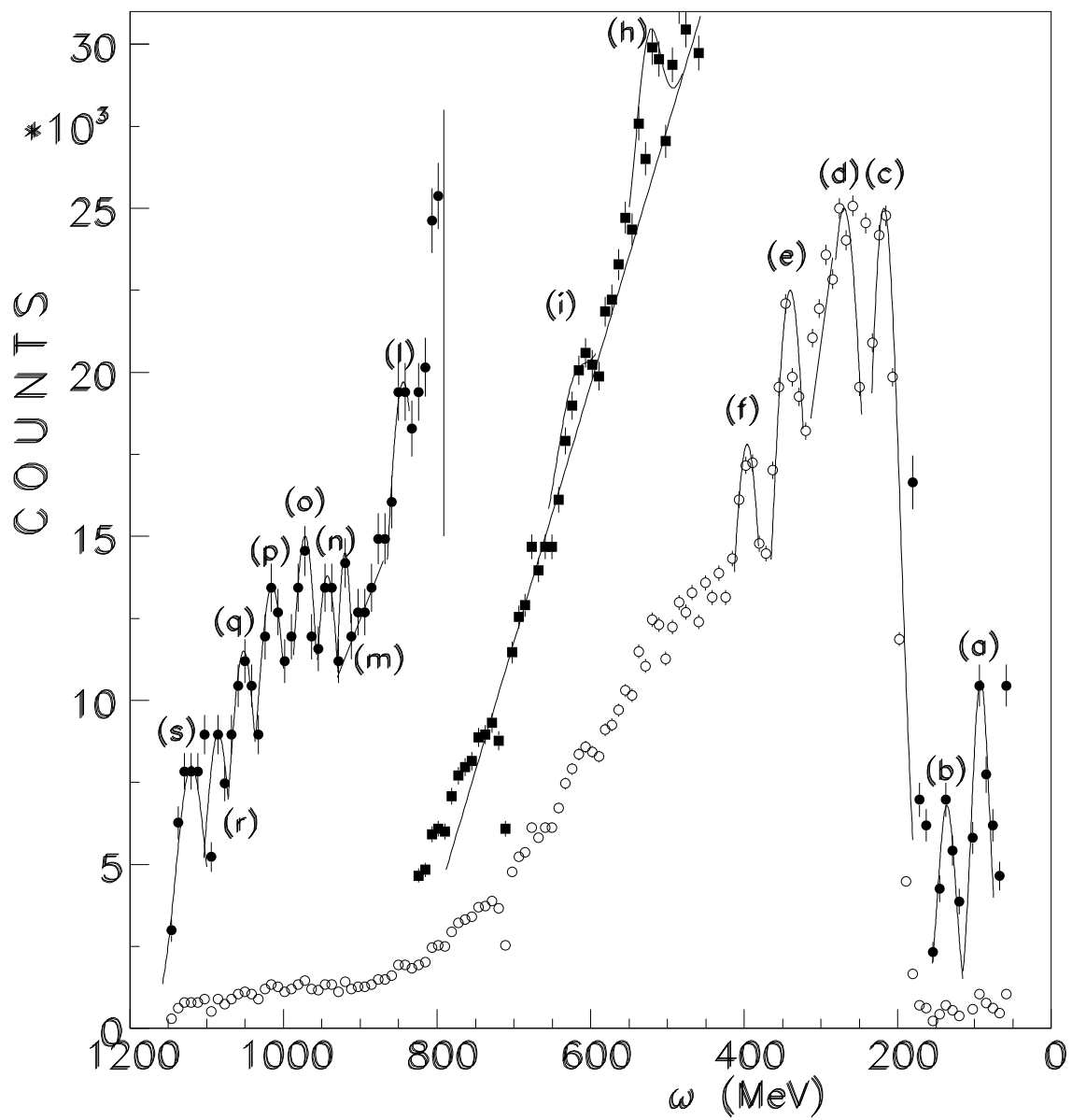


FIG. 3: Same as Fig. 2, but obtained at $\theta=2^\circ$ [12].

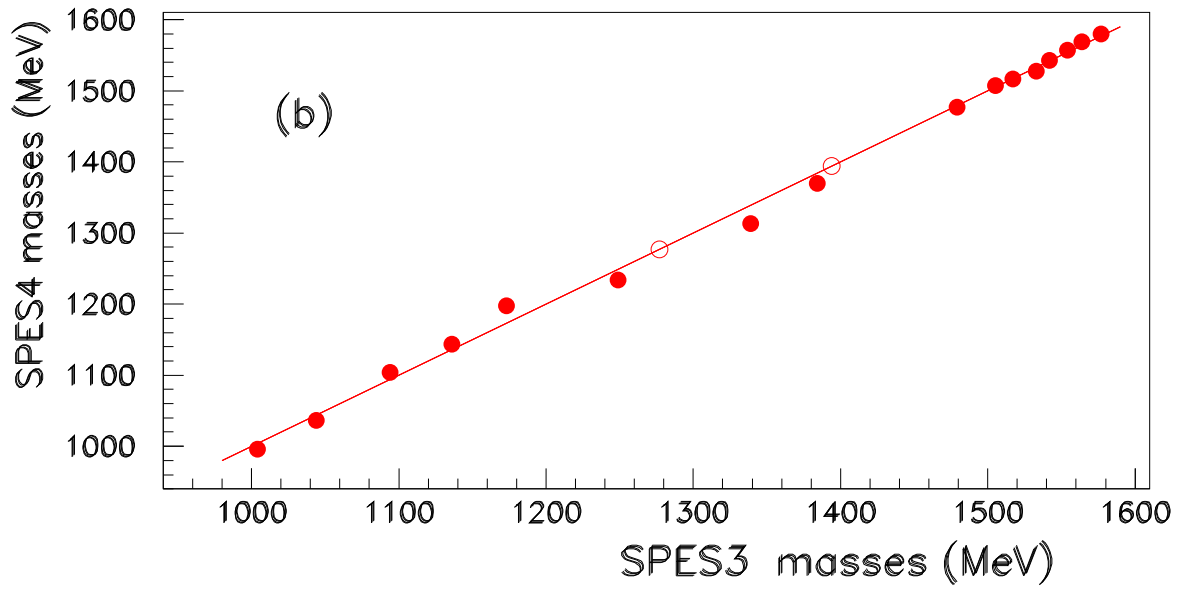
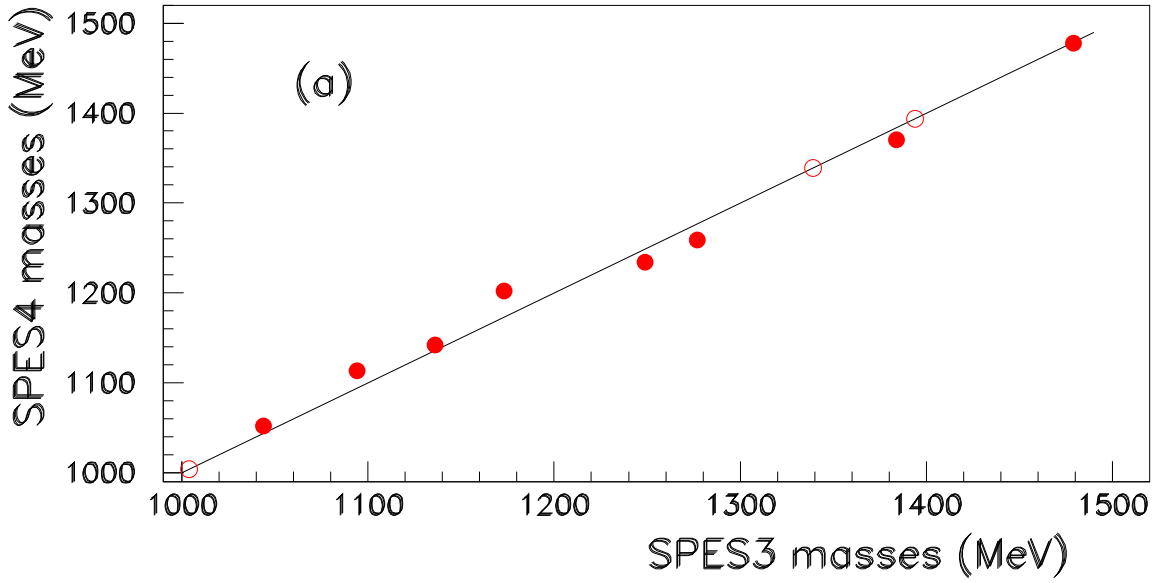


FIG. 4: Comparison between masses of narrow baryons extracted from SPES3 and SPES4 data. Inserts (a) and (b) correspond respectively to $\theta=0.8^\circ$ and $\theta=2^\circ$. Full circles correspond to narrow structure masses observed in both experiments, empty circles correspond to narrow structure masses observed in only one experiment.

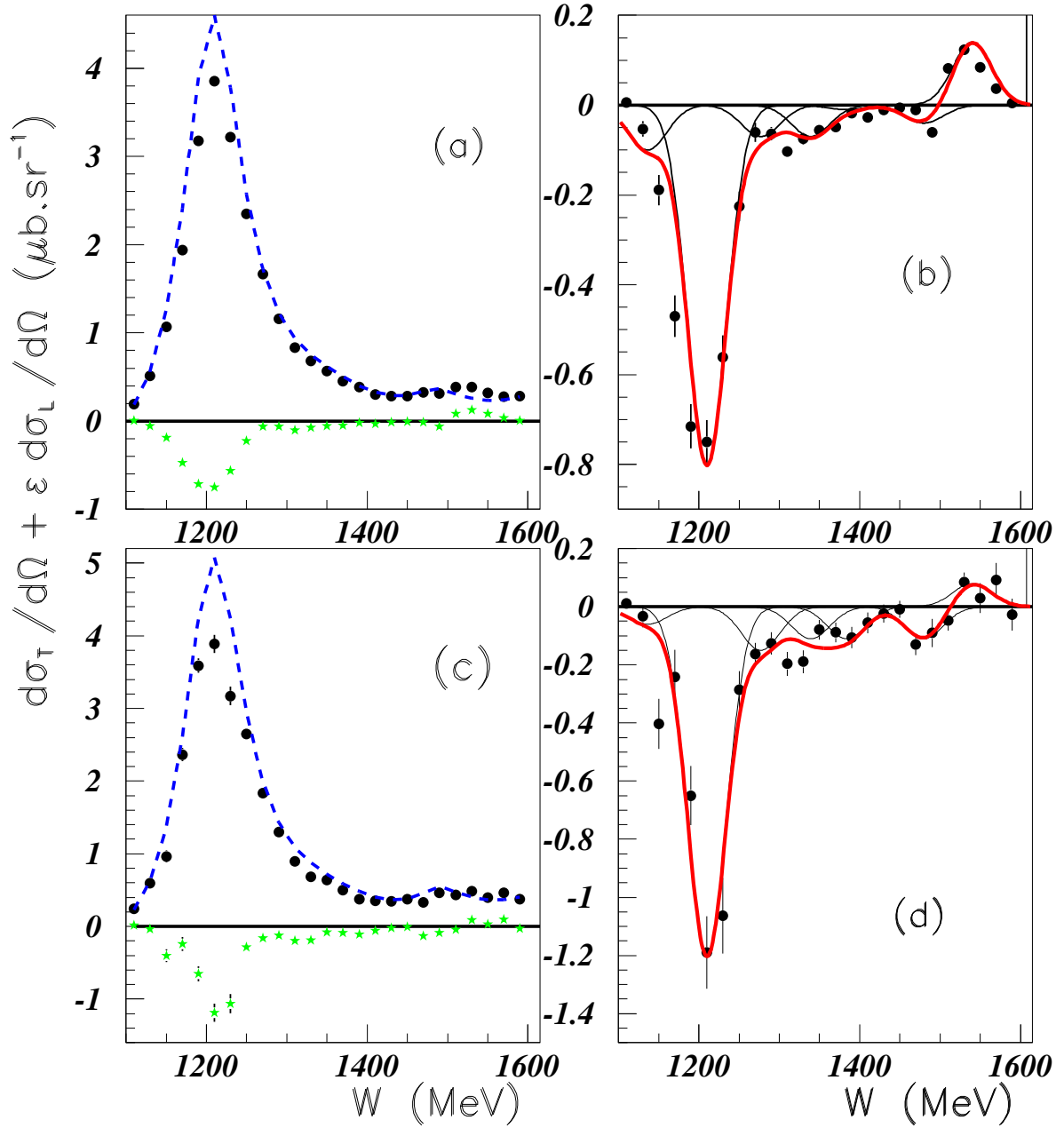


FIG. 5: $\sigma_T + \varepsilon\sigma_L$ structure function of the $\gamma^*p \rightarrow \pi^0p$ reaction [2], at $\theta=167.16^\circ$ in inserts (a) and (b) and at $\theta=157.67^\circ$ in inserts (c) and (d) (see text).

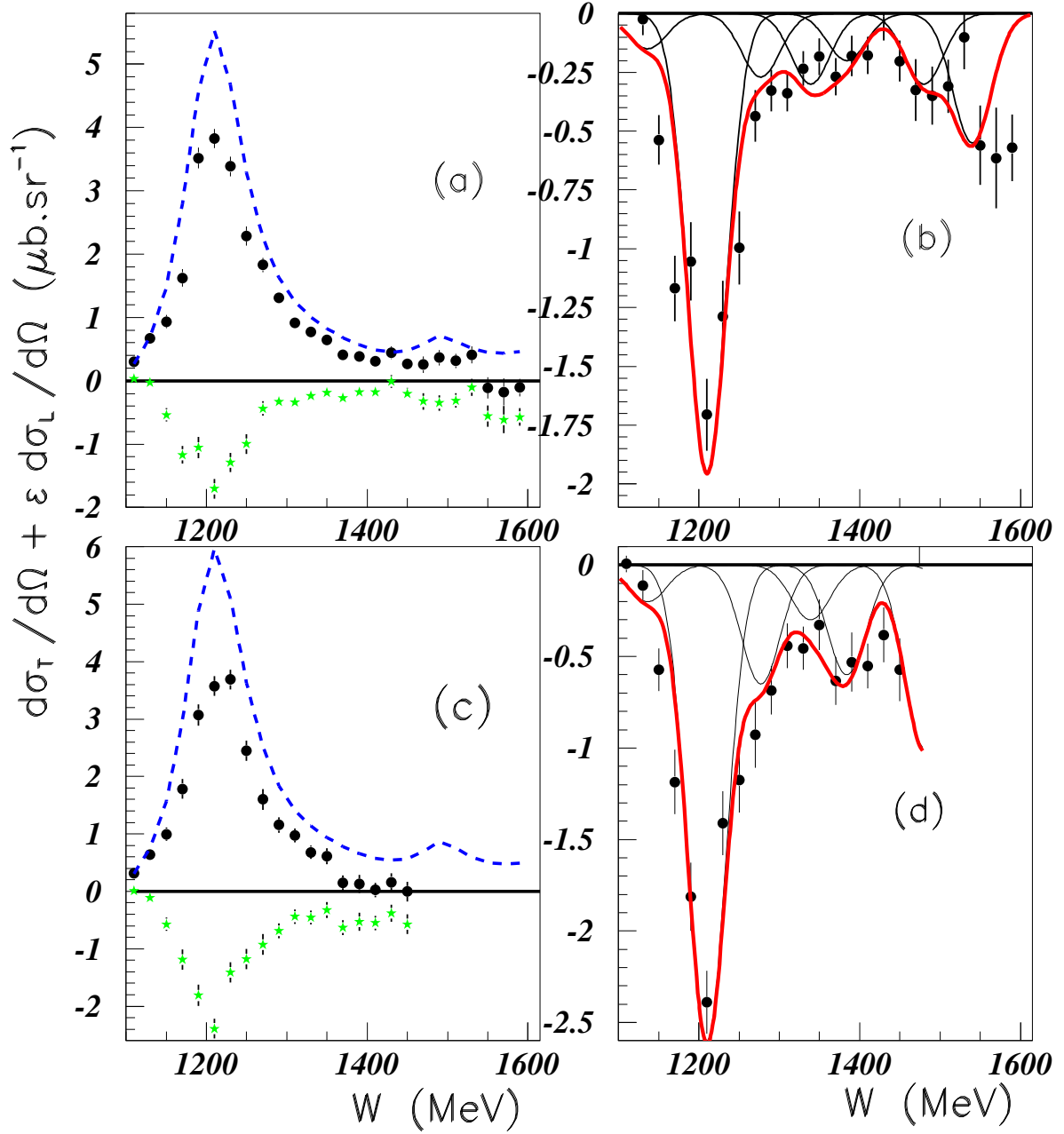


FIG. 6: $\sigma_T + \epsilon\sigma_L$ structure function of the $\gamma^*p \rightarrow \pi^0p$ reaction [2], at $\theta=151.05^\circ$ in inserts (a) and (b) and at $\theta=145.59^\circ$ in inserts (c) and (d) (see text).

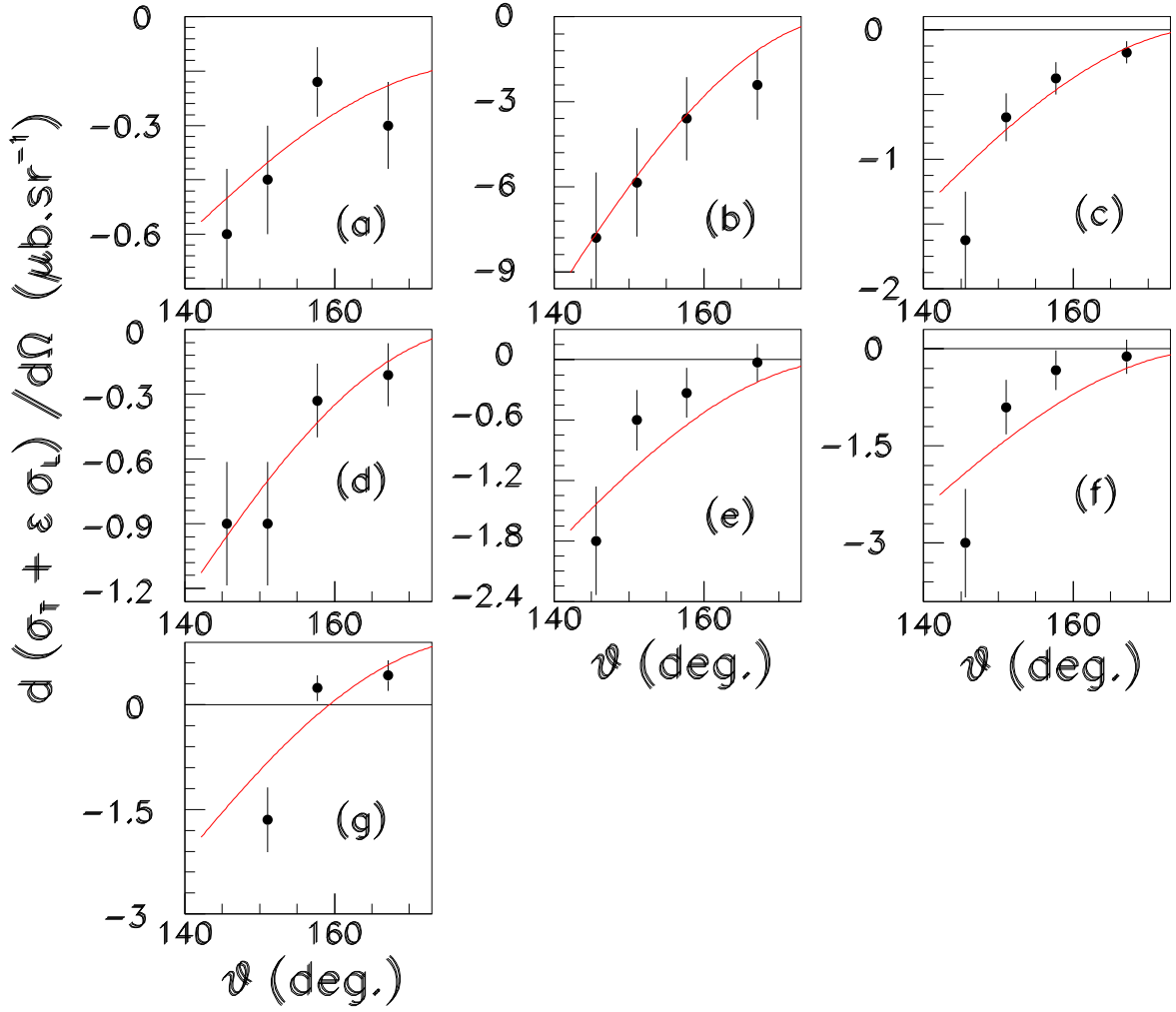


FIG. 7: Angular variations of the $\sigma_T + \epsilon\sigma_L$ structure function for the seven narrow structure masses as extracted from Figs. 1 and 2. (see text). Inserts (a), (b), (c), (d), (e), (f), and (g) correspond respectively to the following masses: $M=1136$ MeV, 1210 MeV, 1277 MeV, 1339 MeV, 1384 MeV, 1480 MeV, and 1540 MeV.

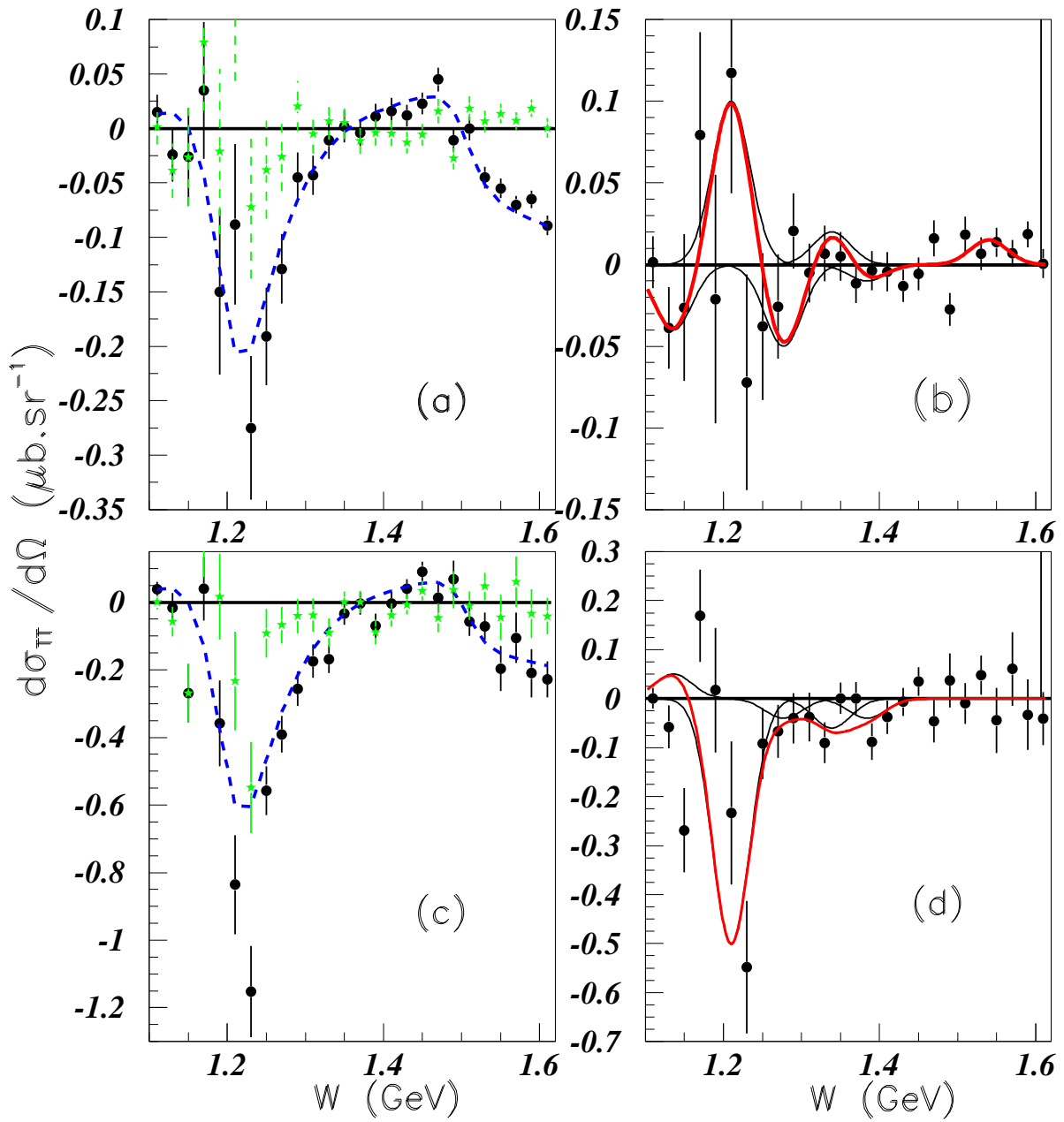


FIG. 8: Same as in Fig. 5 but for σ_{TT} structure function.

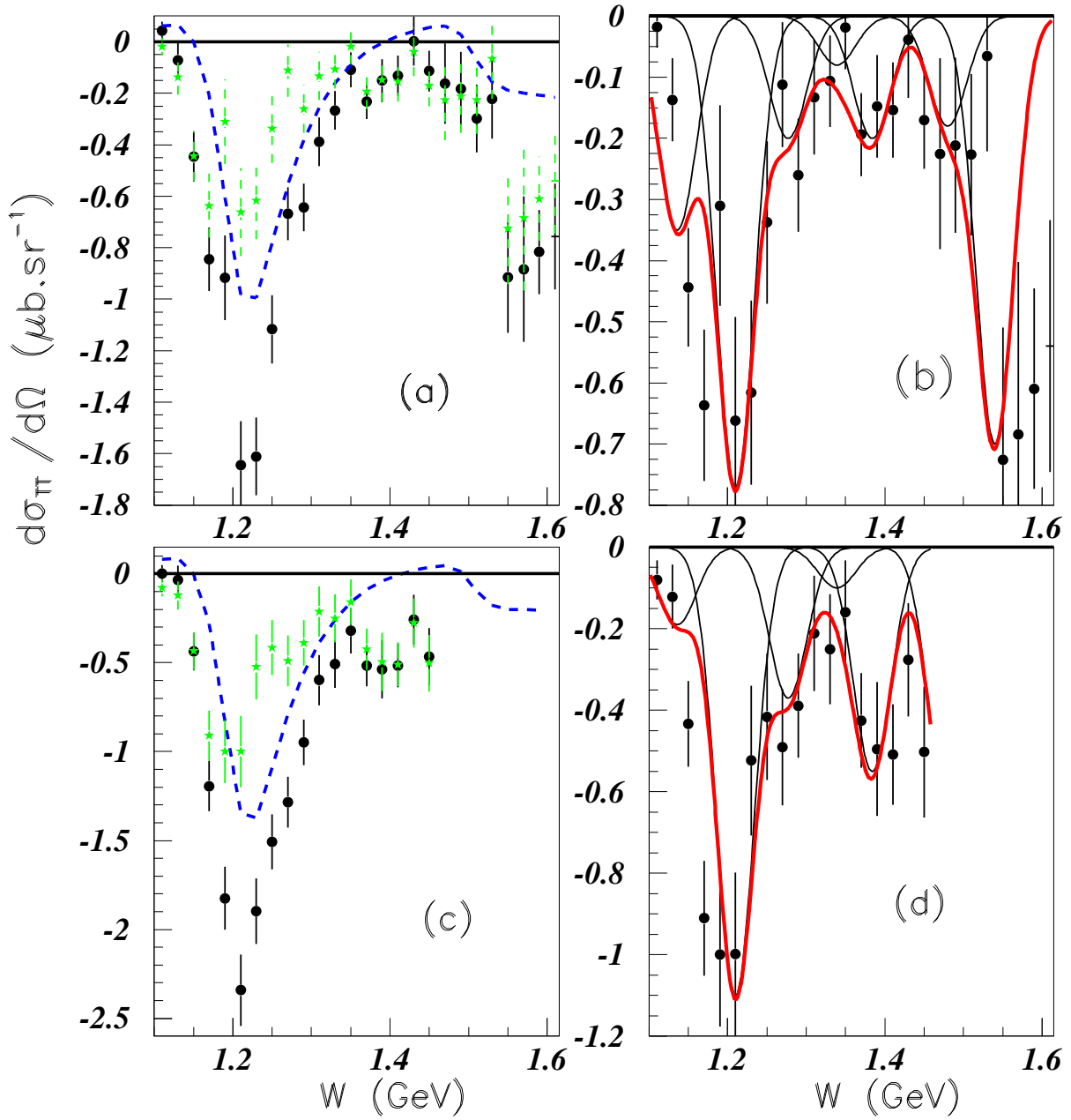


FIG. 9: Same as in Fig. 6 but for σ_{TT} structure function.

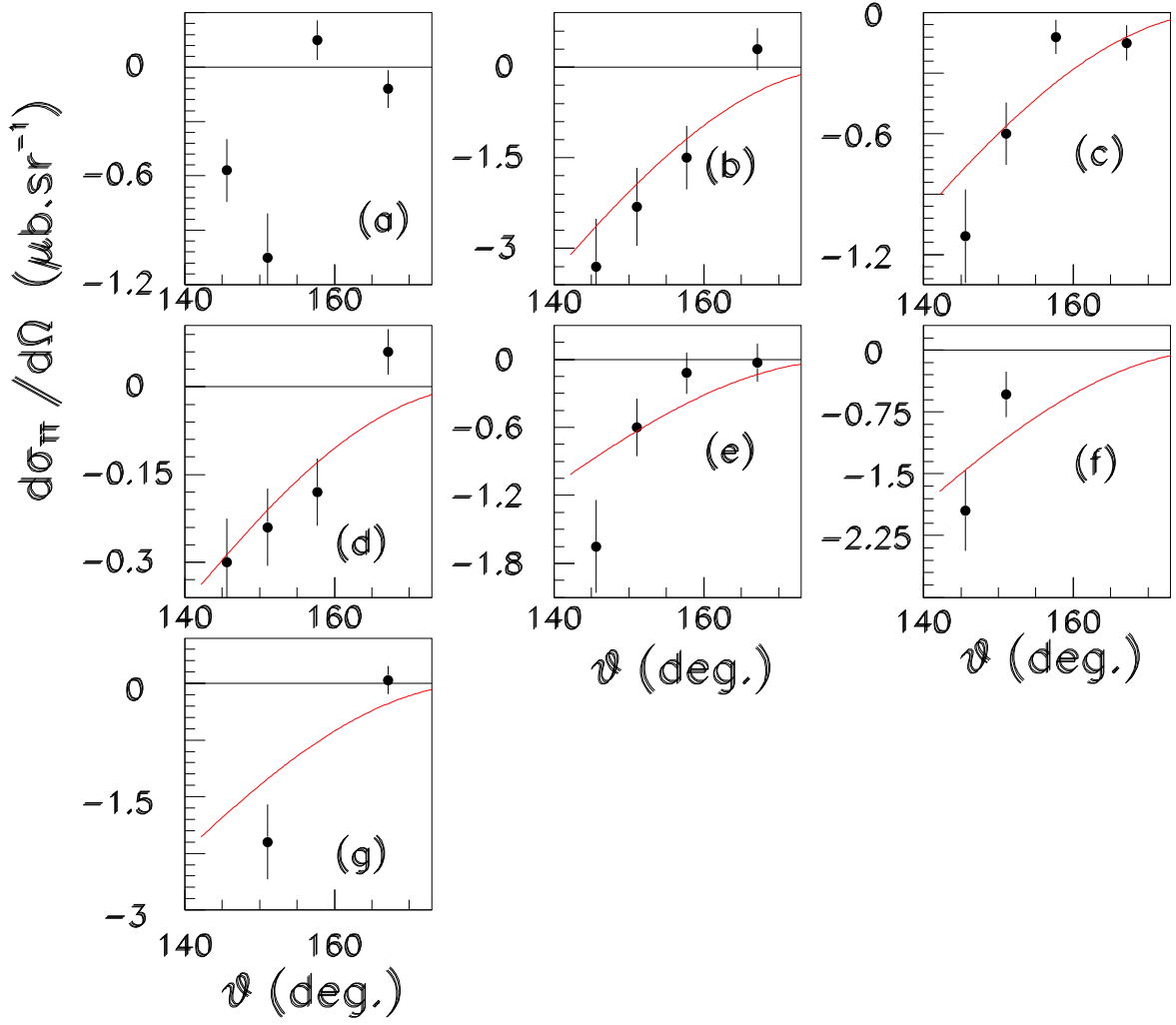


FIG. 10: Angular variations of σ_{TT} structure function for the seven narrow structure masses as extracted from Figs. 8 and 9 (see text). Inserts (a), (b), (c), (d), (e), (f), and (g) correspond respectively to the following masses: $M=1136$ MeV, 1210 MeV, 1277 MeV, 1339 MeV, 1384 MeV, 1480 MeV, and 1540 MeV.

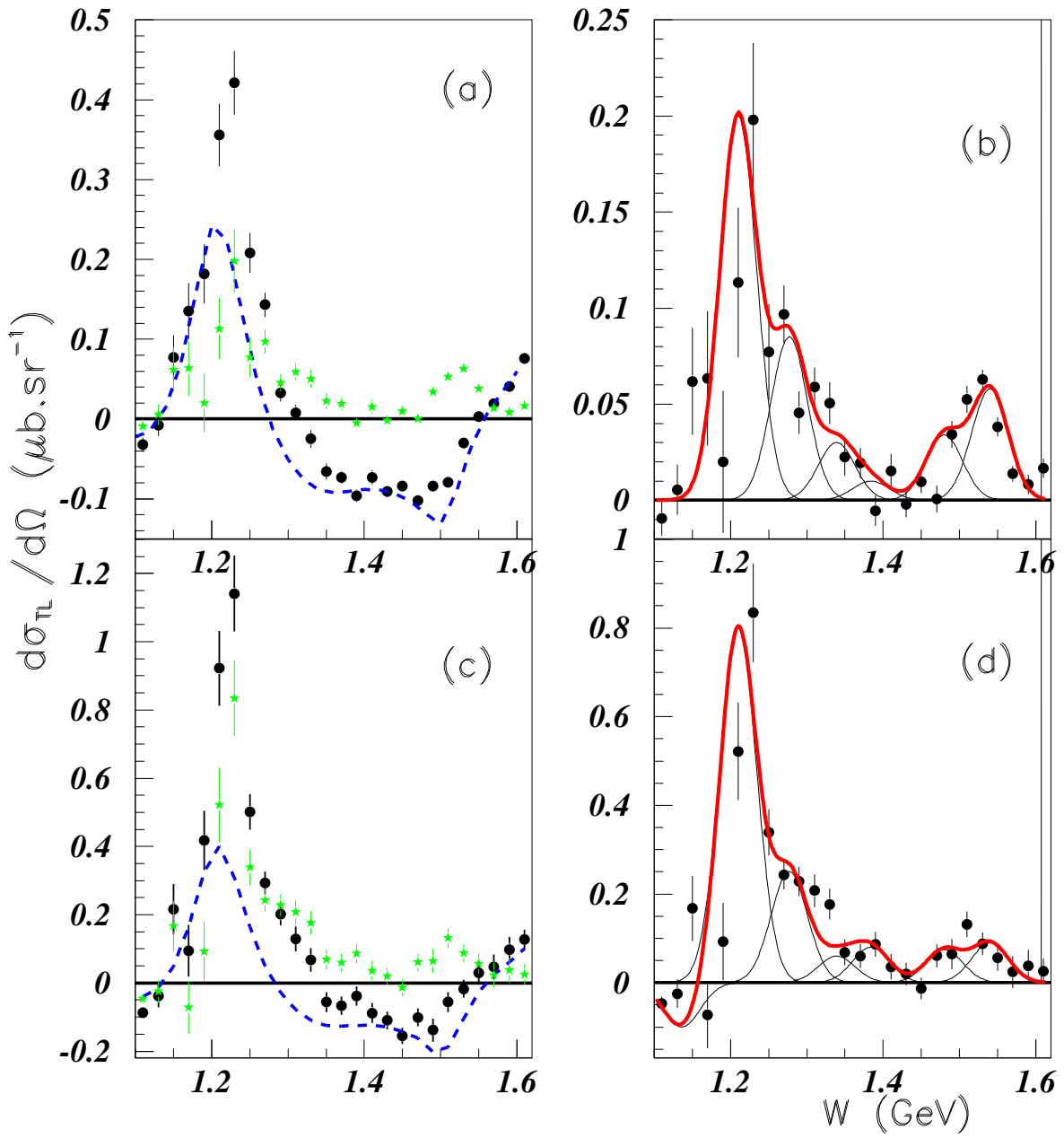


FIG. 11: Same as in Fig. 5 but for σ_{TL} structure function.

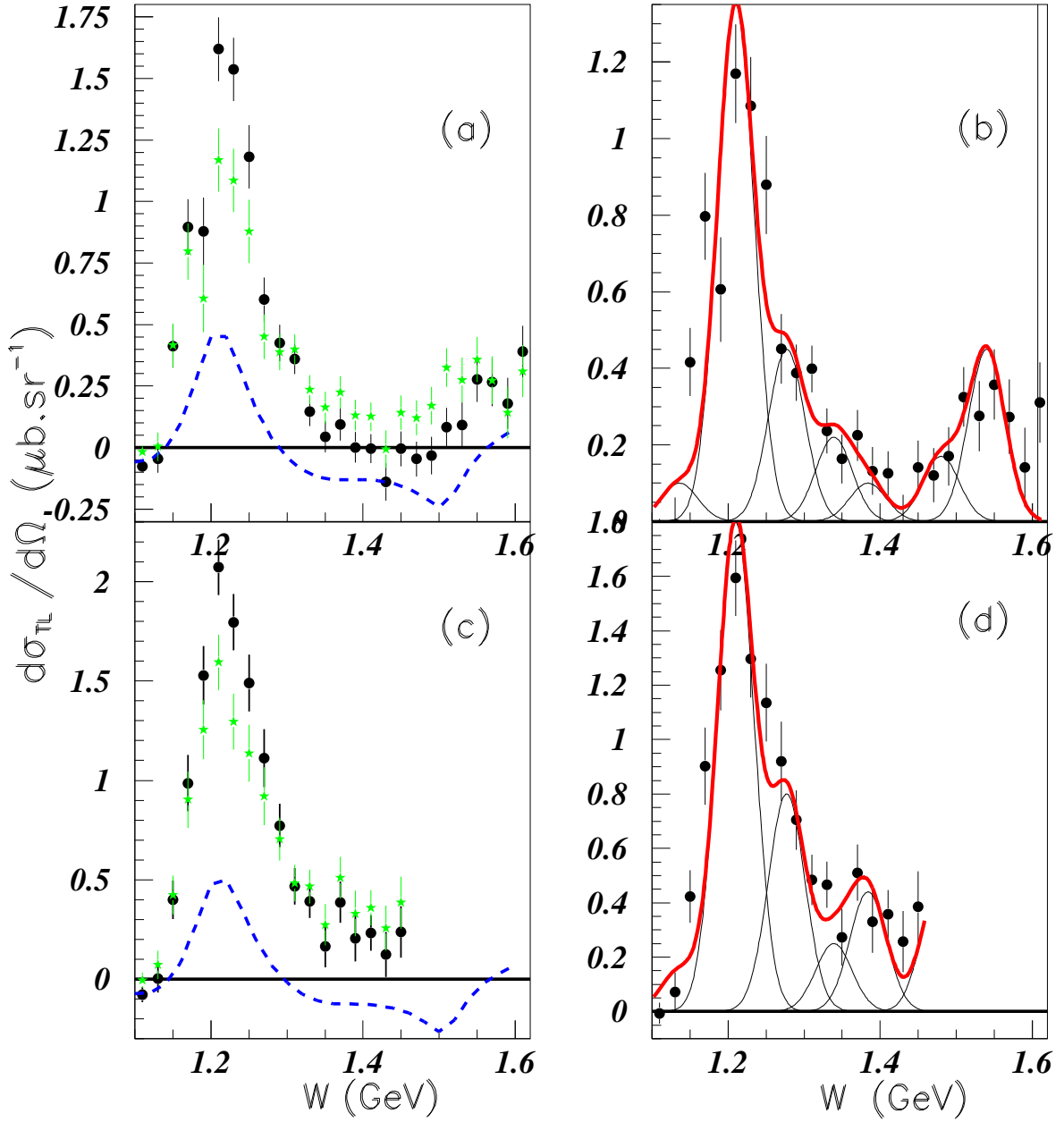


FIG. 12: Same as in Fig. 6 but for σ_{TL} structure function.

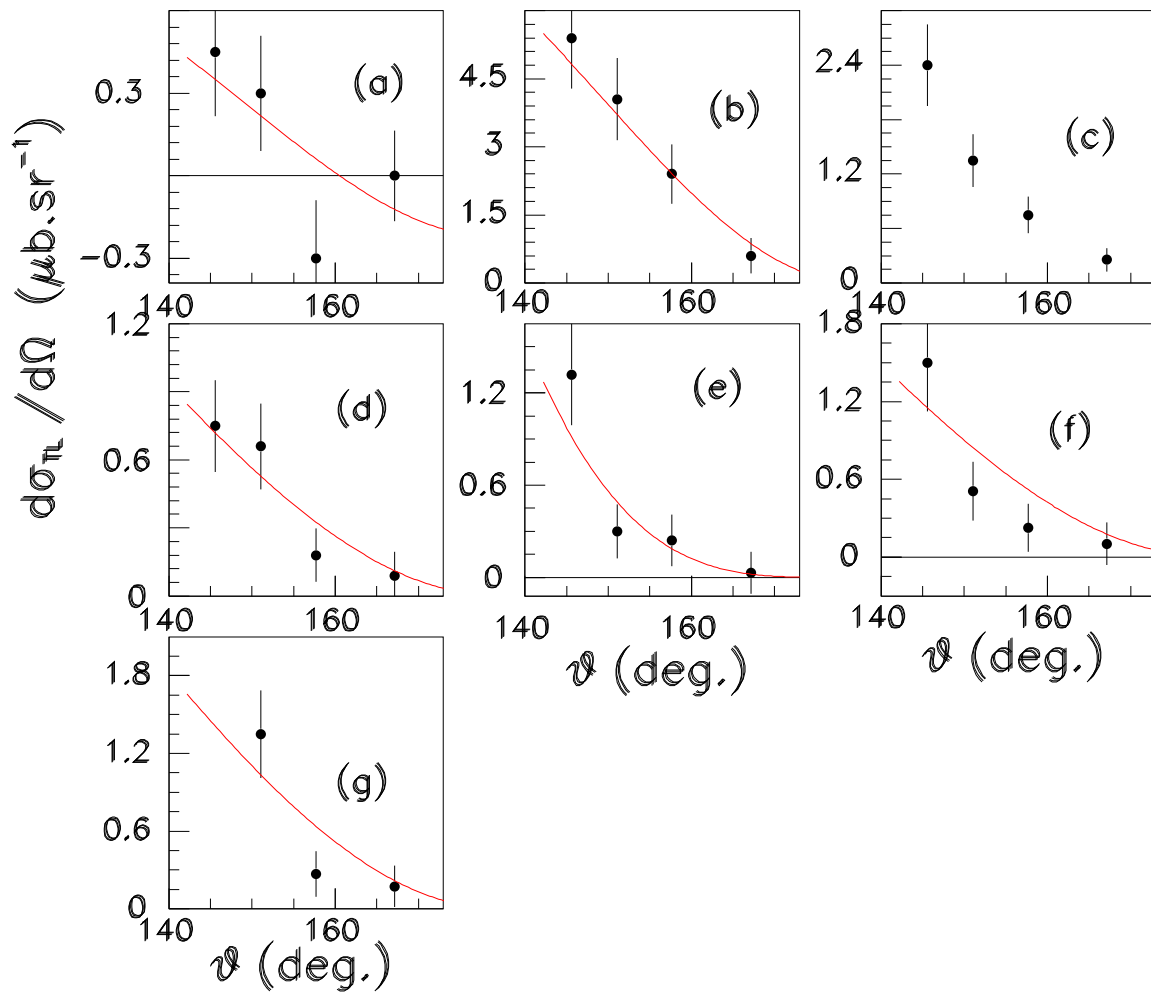


FIG. 13: Same as in Fig. 7, but for σ_{TL} structure function.

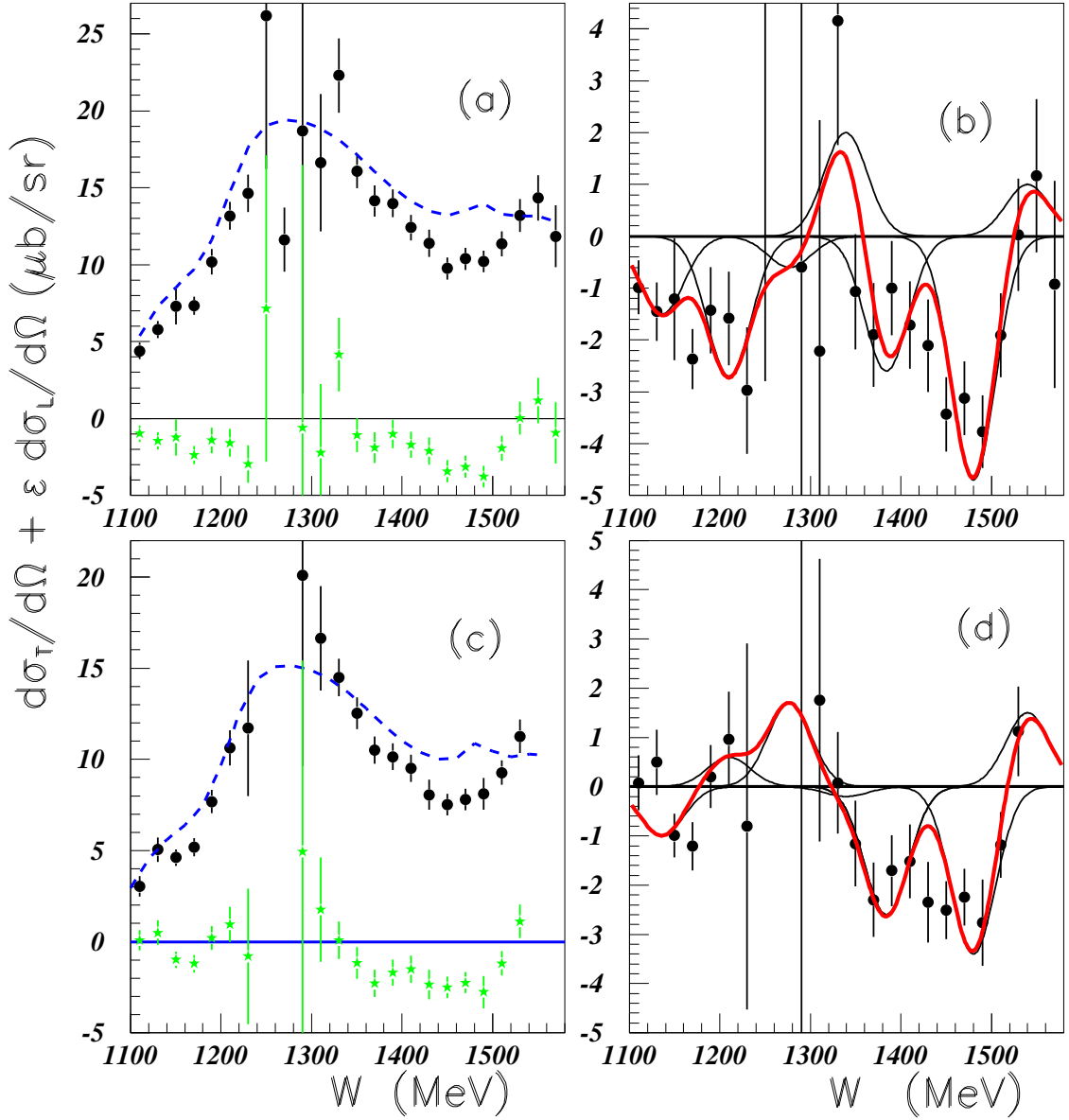


FIG. 14: $\sigma_T + \epsilon\sigma_L$ structure function of the $\gamma^*p \rightarrow \pi^+n$ reaction [3], at $\theta=7.5^\circ$ and $Q^2=0.3 \text{ GeV}^2$ in inserts (a) and (b) and at $\theta=7.5^\circ$ and $Q^2=0.4 \text{ GeV}^2$ in inserts (c) and (d) (see text).

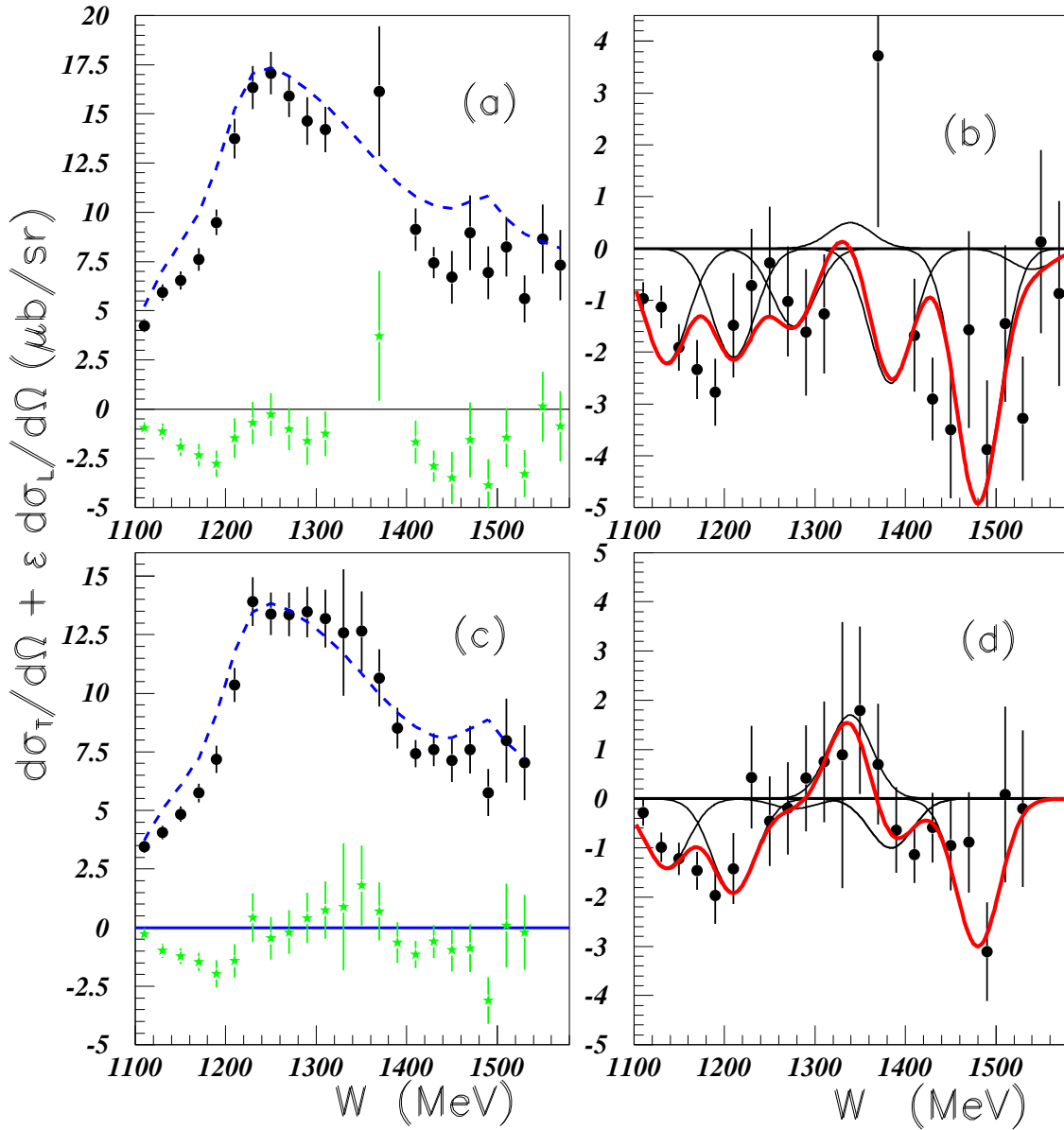


FIG. 15: Same as in Fig. 14 but for $\theta=22.5^\circ$.

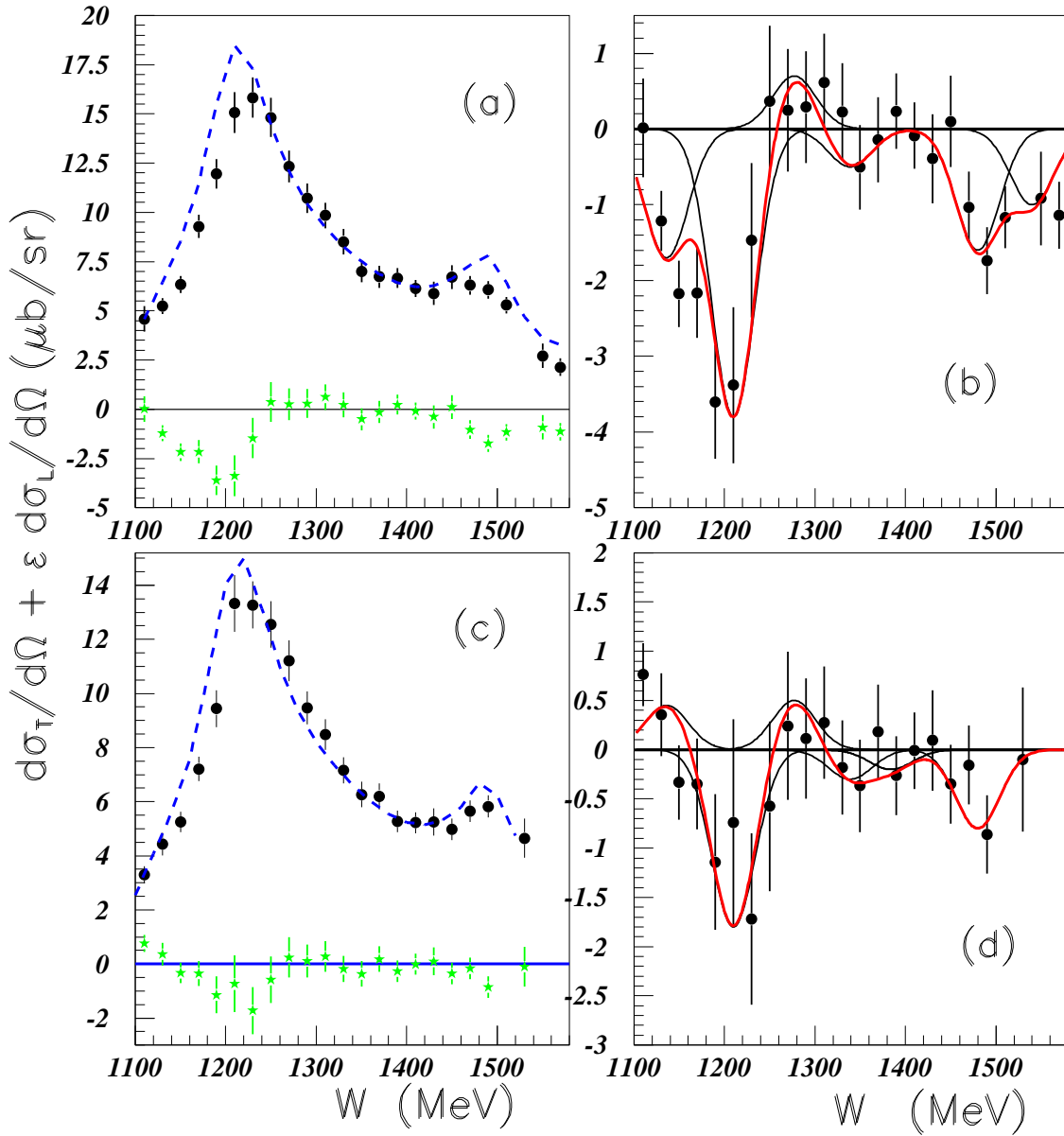


FIG. 16: Same as in Fig. 14 but for $\theta=52.5^\circ$.

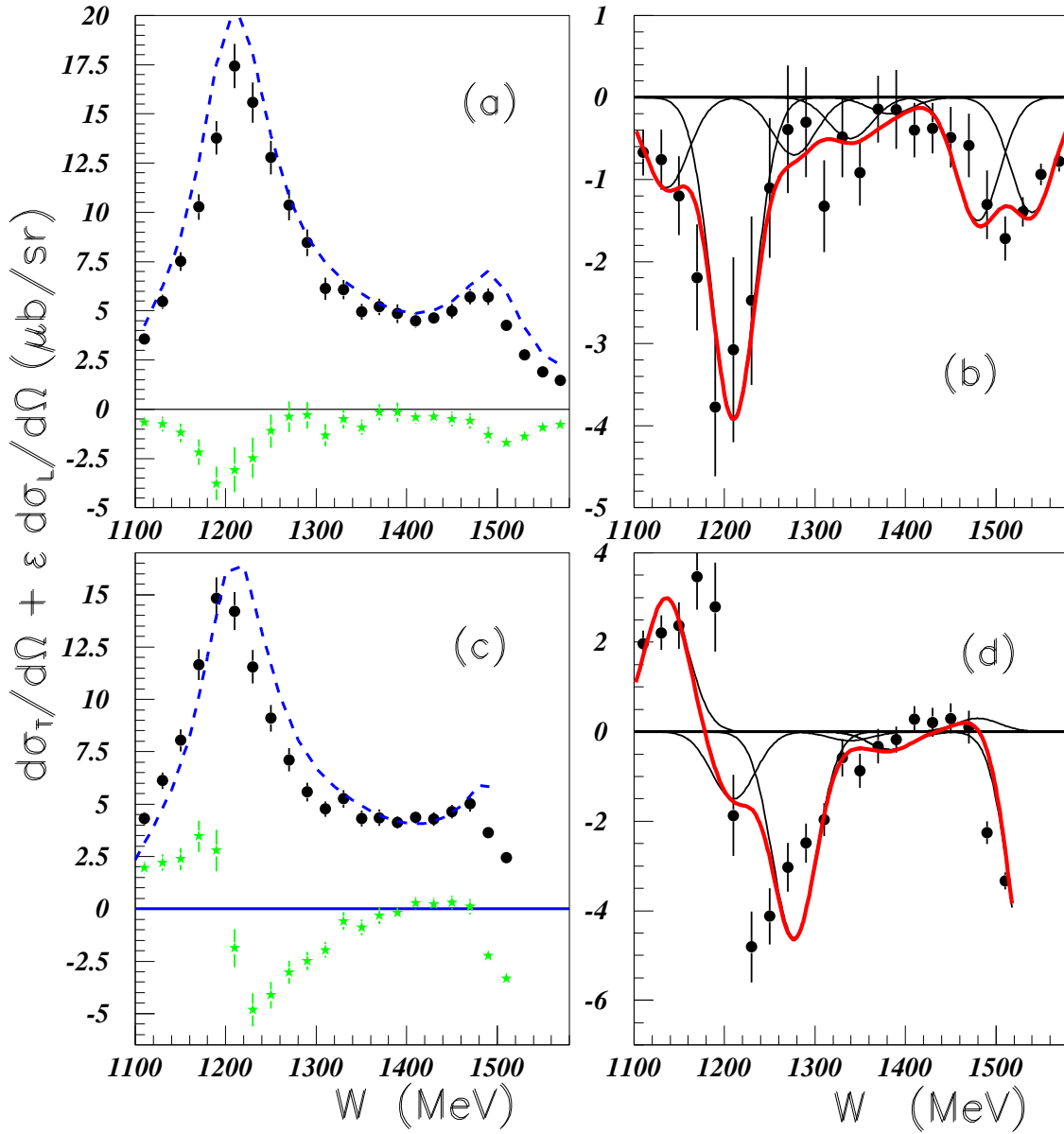


FIG. 17: Same as in Fig. 14 but for $\theta=67.5^\circ$.

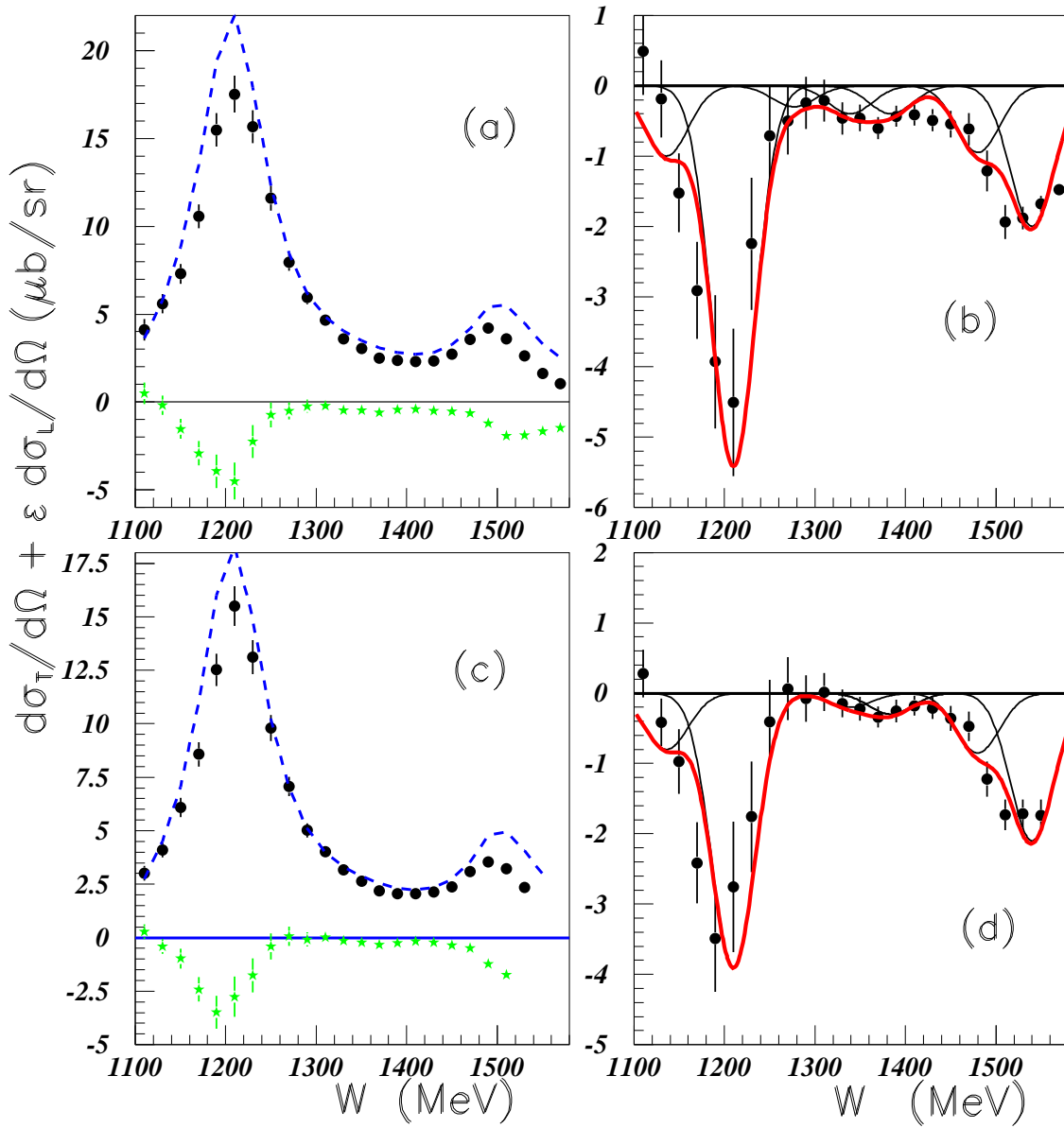


FIG. 18: Same as in Fig. 14 but for $\theta=97.5^\circ$.

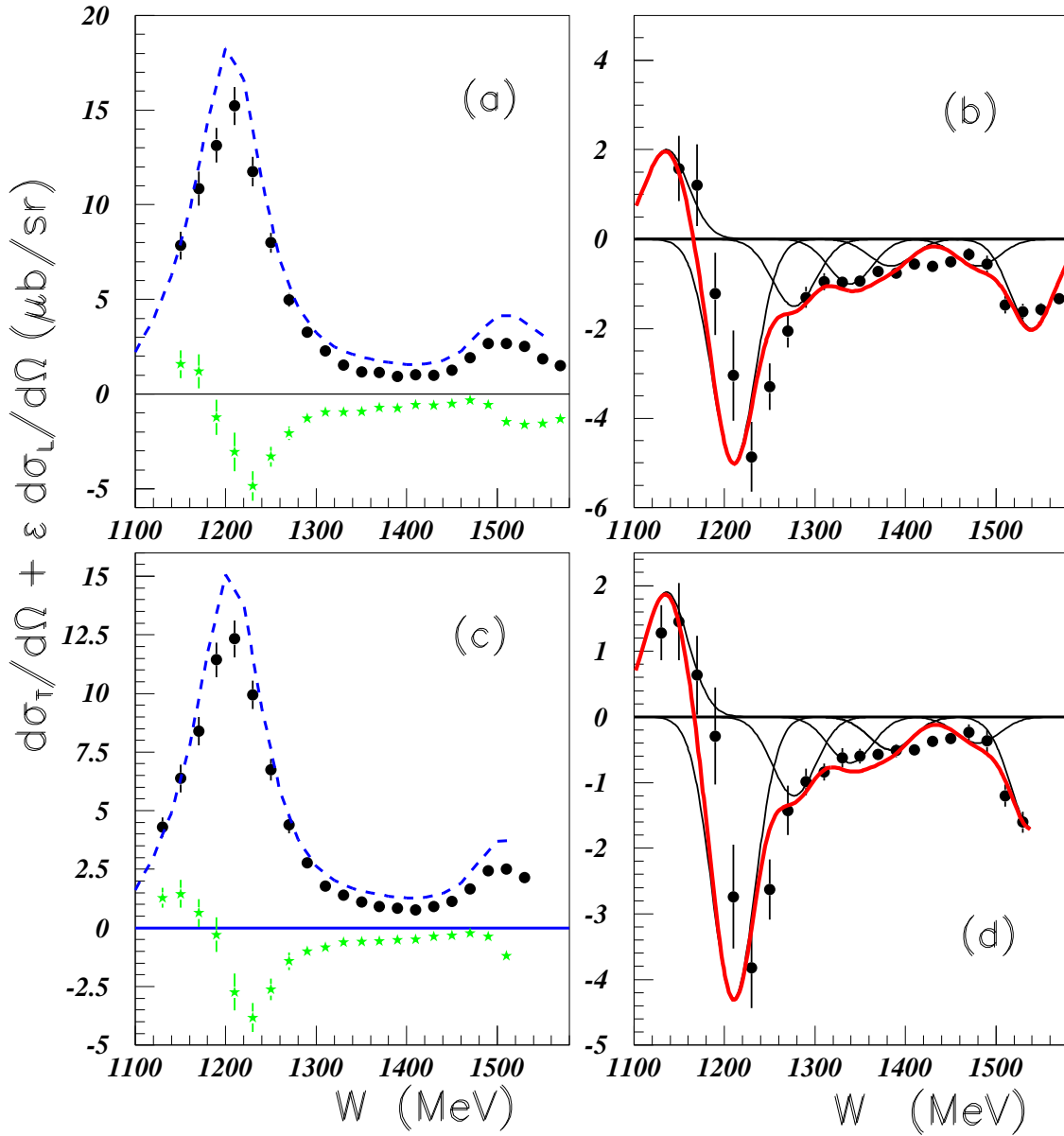


FIG. 19: Same as in Fig. 14 but for $\theta=127.5^\circ$.

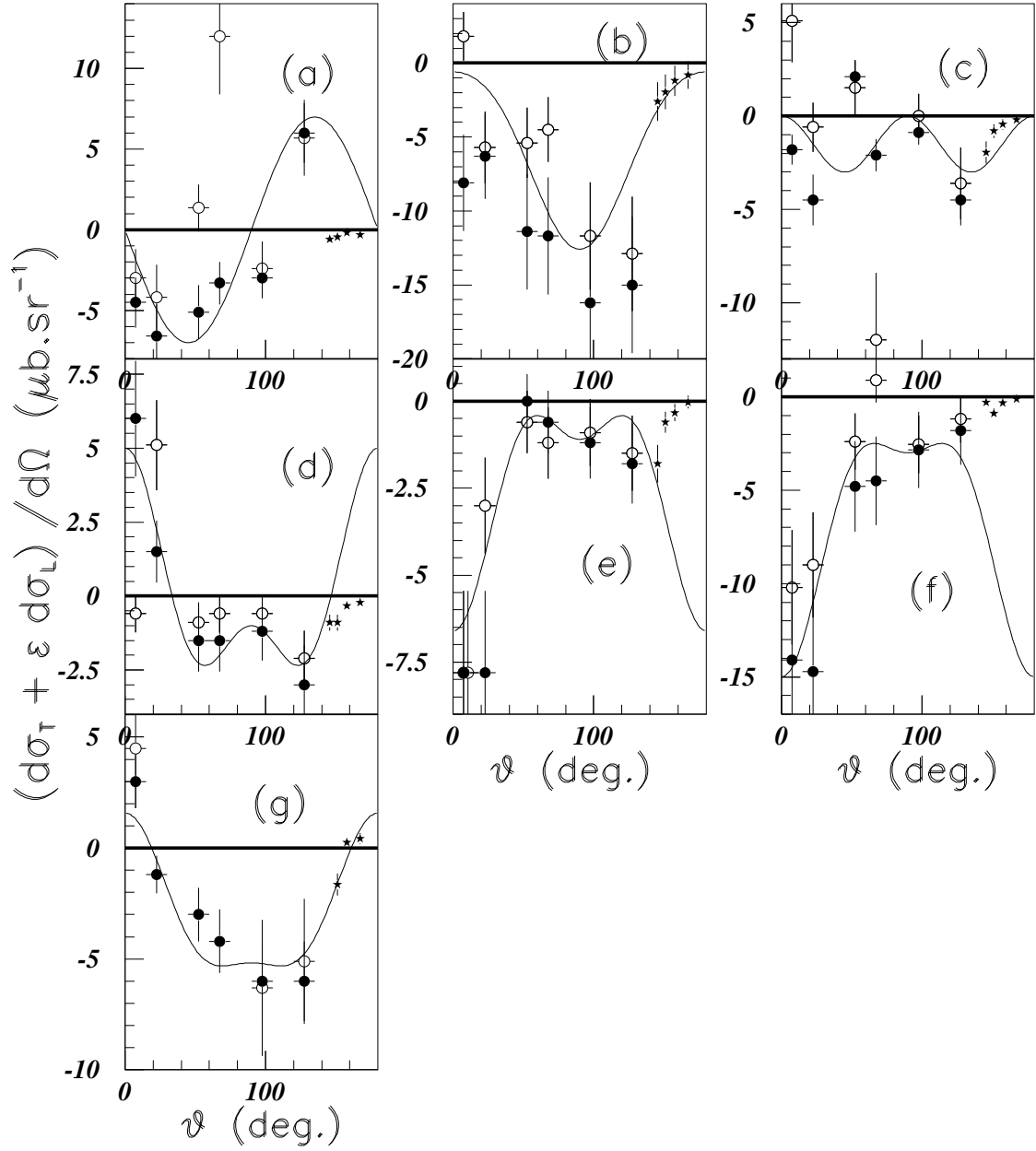


FIG. 20: Same as in Fig. 7 but showing the angular variation of the yield of the $\sigma_T + \epsilon\sigma_L$ structure function for both reactions. Full circles correspond to $Q^2=0.3 \text{ GeV}^2$, empty circles correspond to $Q^2=0.4 \text{ GeV}^2$, and stars correspond to $Q^2=1 \text{ GeV}^2$ (see text).

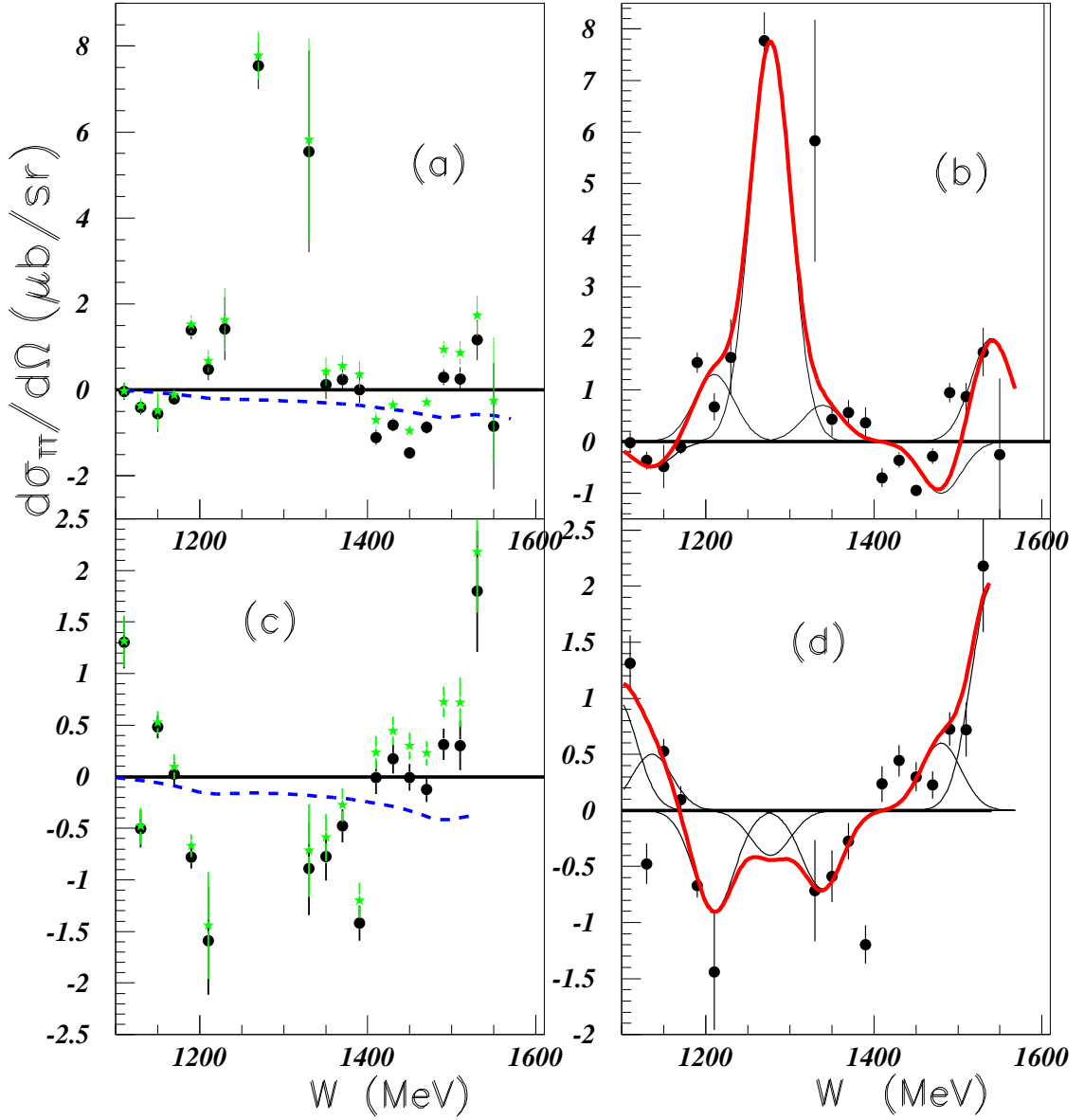


FIG. 21: Cross-section of the σ_{TT} structure function of the $ep \rightarrow e'n\pi^+$ reaction at $\theta=7.5^\circ$. Inserts (a) and (b) show the results at $Q^2=0.3 \text{ GeV}^2$, inserts (c) and (d) show the results at $Q^2=0.4 \text{ GeV}^2$.

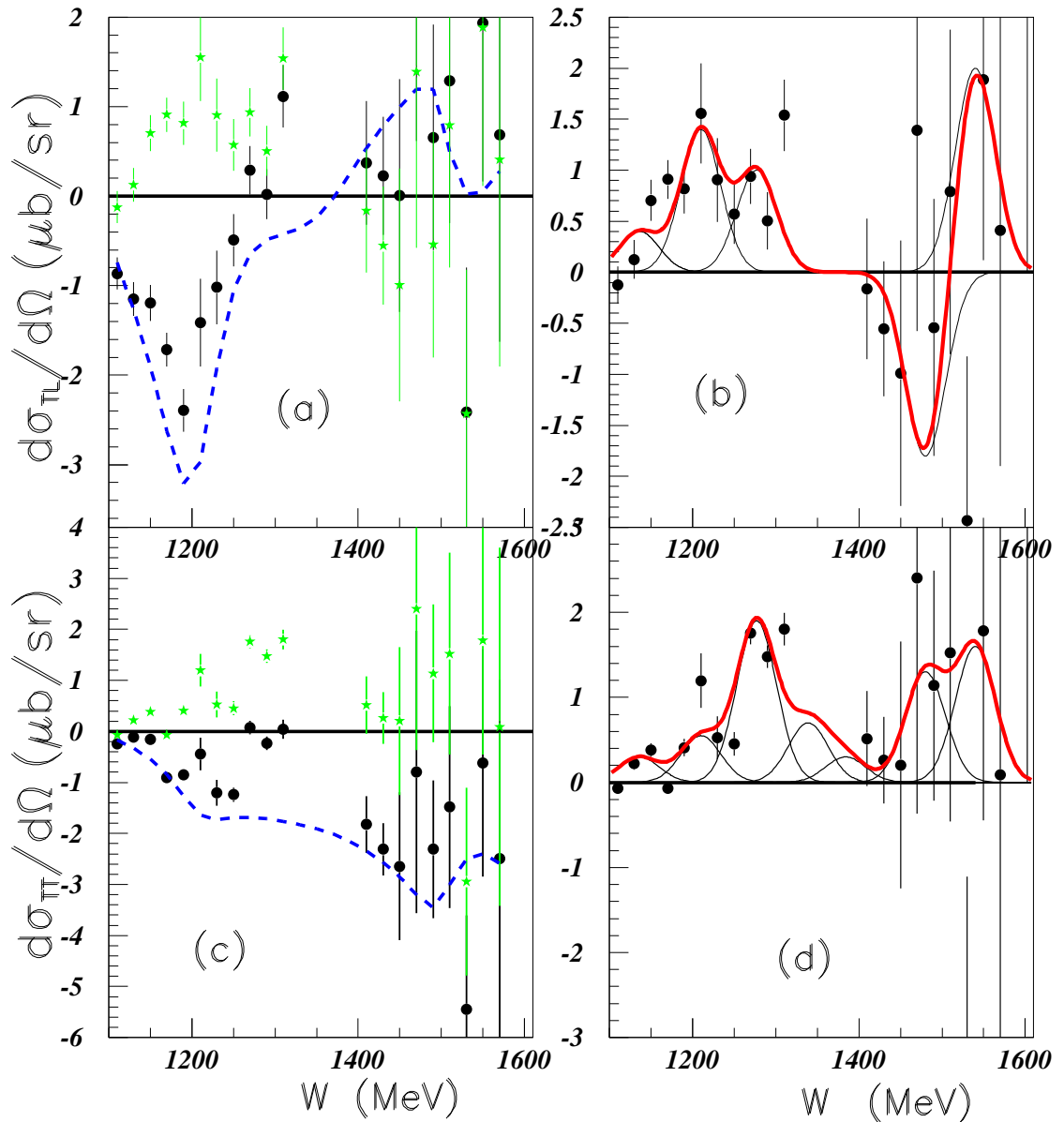


FIG. 22: Cross-section of two structure functions of the $ep \rightarrow e'n\pi^+$ reaction at $\theta=22.5^\circ$ and $Q^2=0.3 \text{ GeV}^2$. Inserts (a) and (b) show the σ_{TL} structure function, and inserts (c) and (d) show the σ_{TT} structure function.

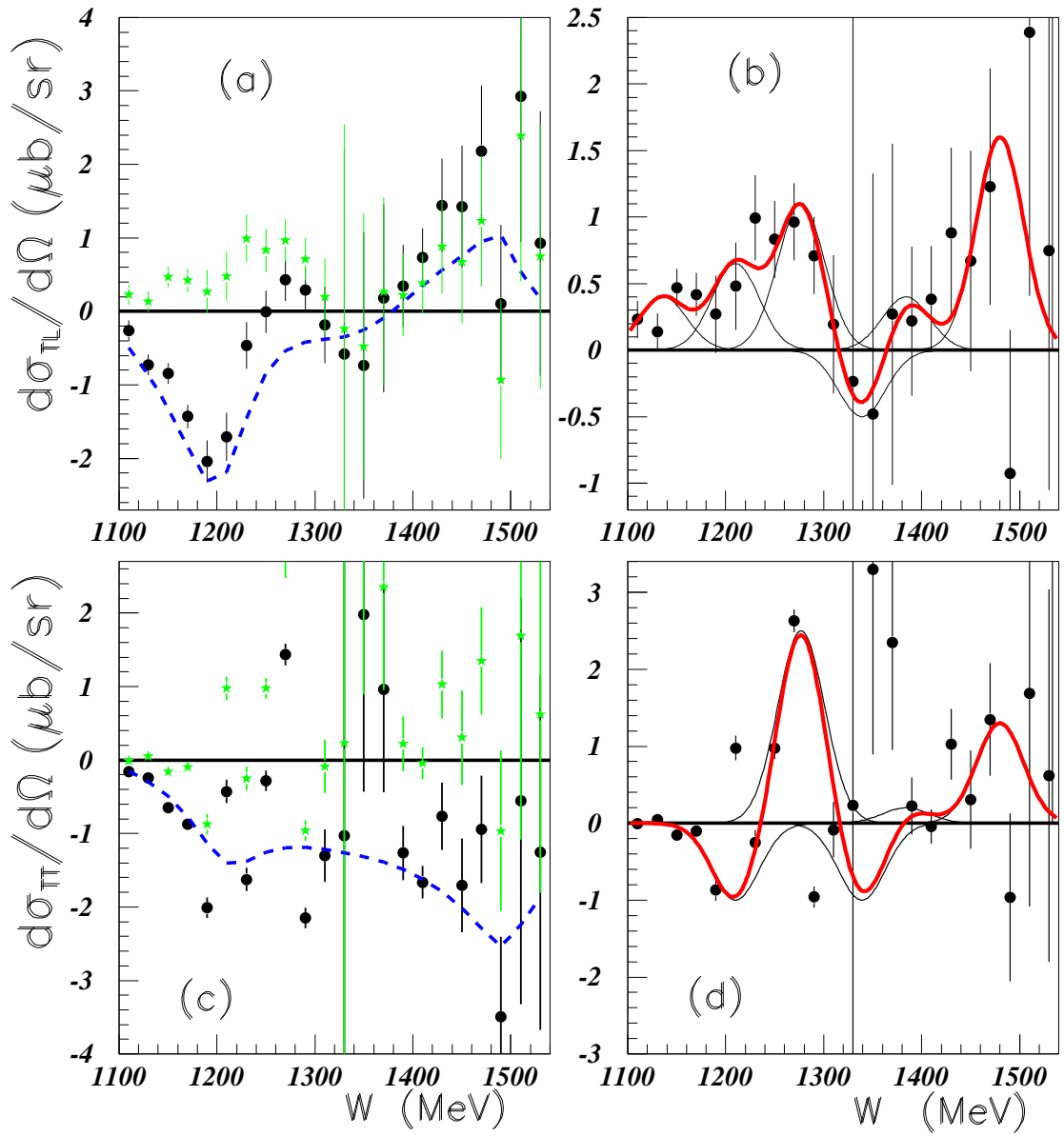


FIG. 23: Same as in Fig. 22 but for $Q^2=0.4 \text{ GeV}^2$.

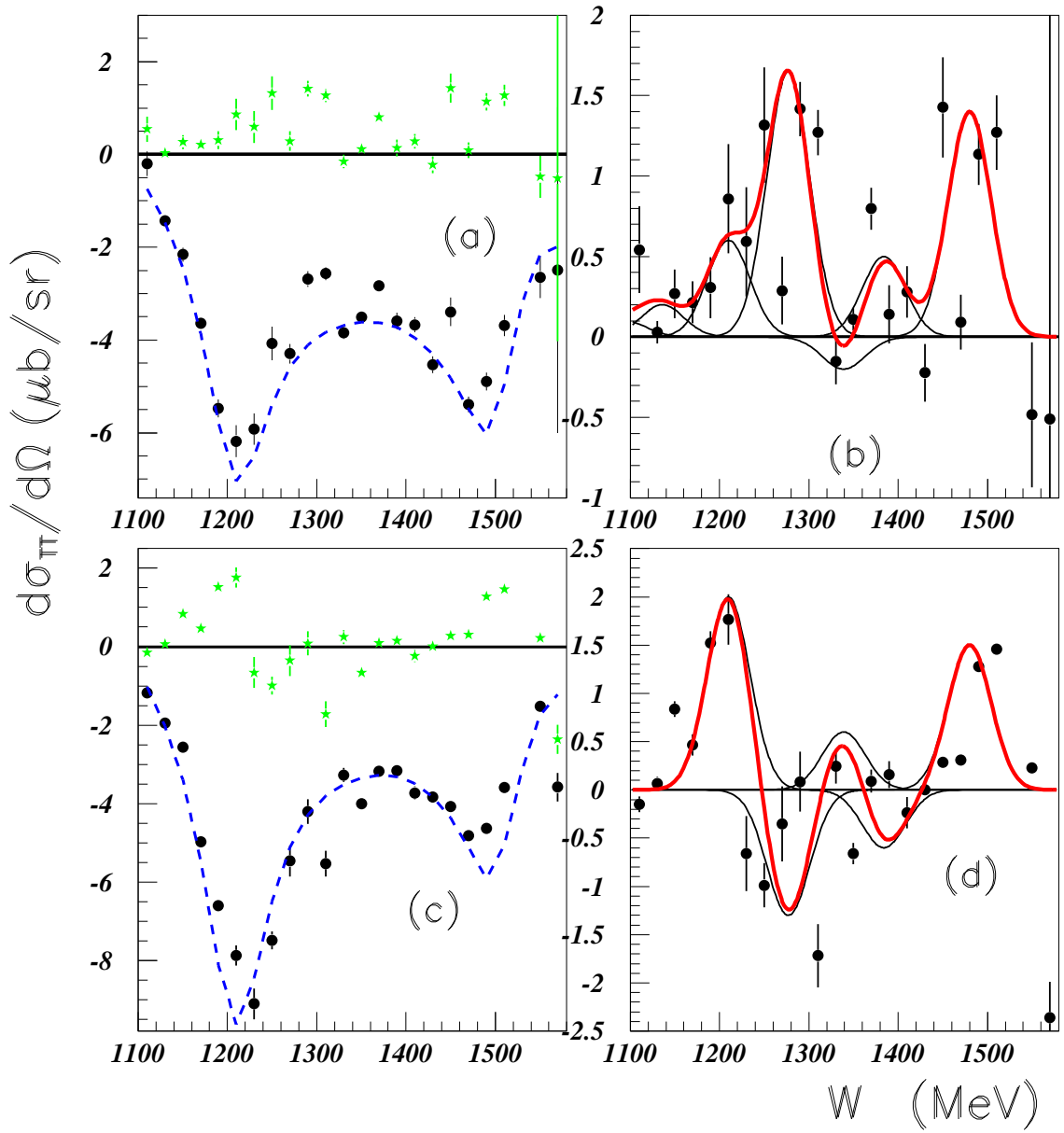


FIG. 24: Cross-section of the σ_{TT} structure function of the $ep \rightarrow e'n\pi^+$ reaction at $Q^2=0.3 \text{ GeV}^2$ $\theta=52.5^\circ$ in inserts (a) and (b), and $\theta=67.5^\circ$ in inserts (c) and (d).

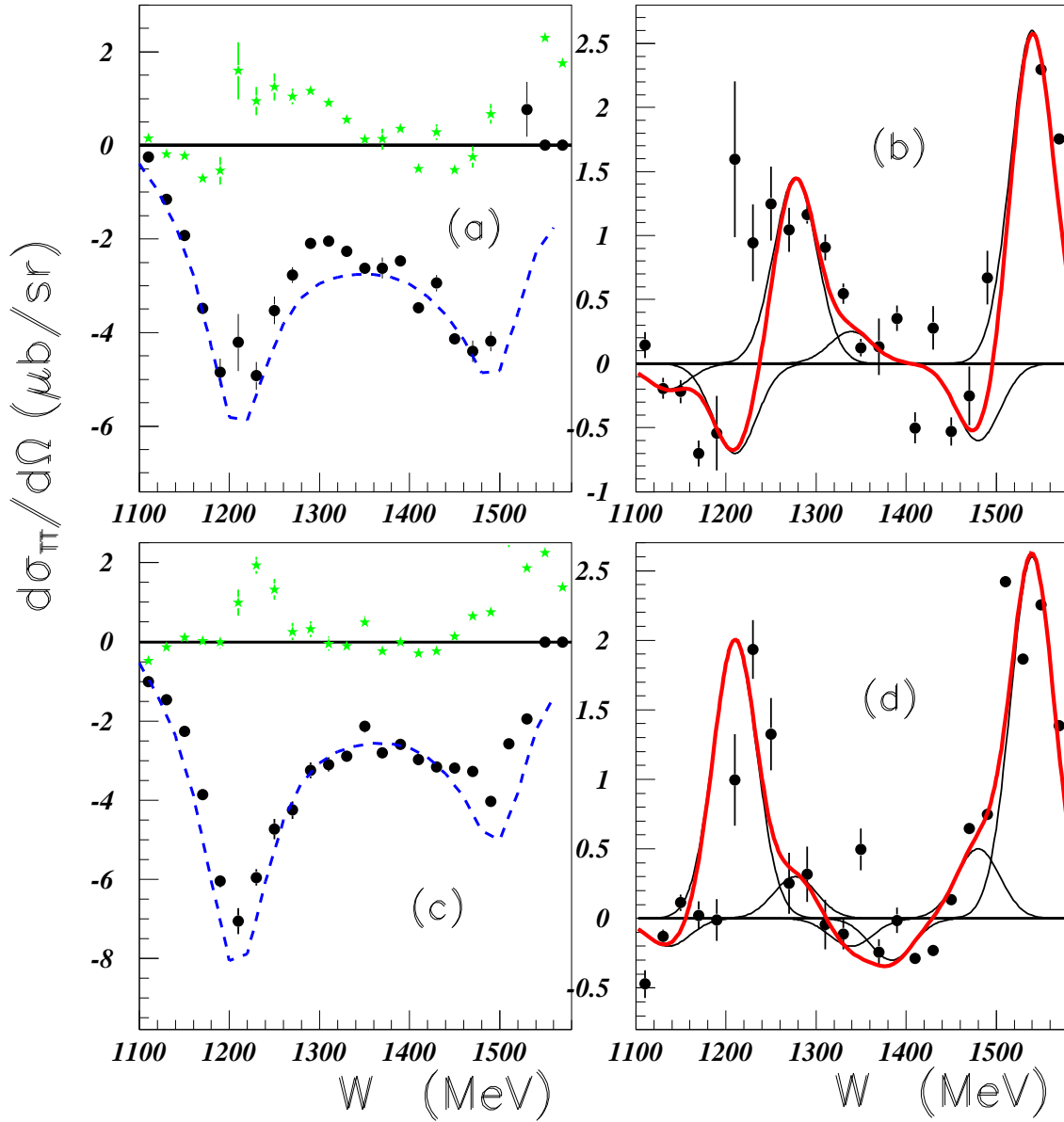


FIG. 25: Same as in Fig. 24, but for $Q^2=0.4 \text{ GeV}^2$.

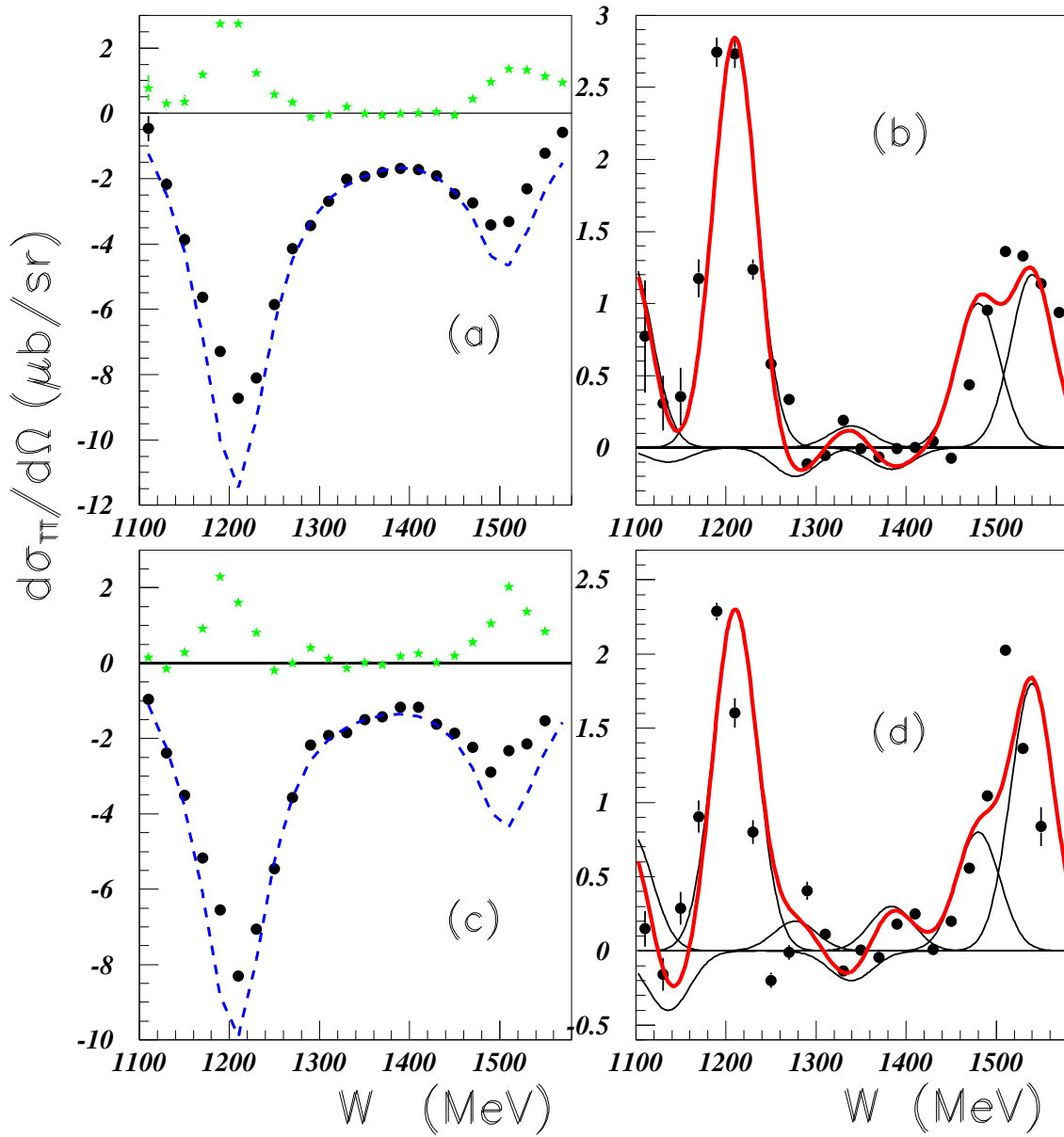


FIG. 26: Same as in Fig. 21, but for $\theta=97.5^\circ$

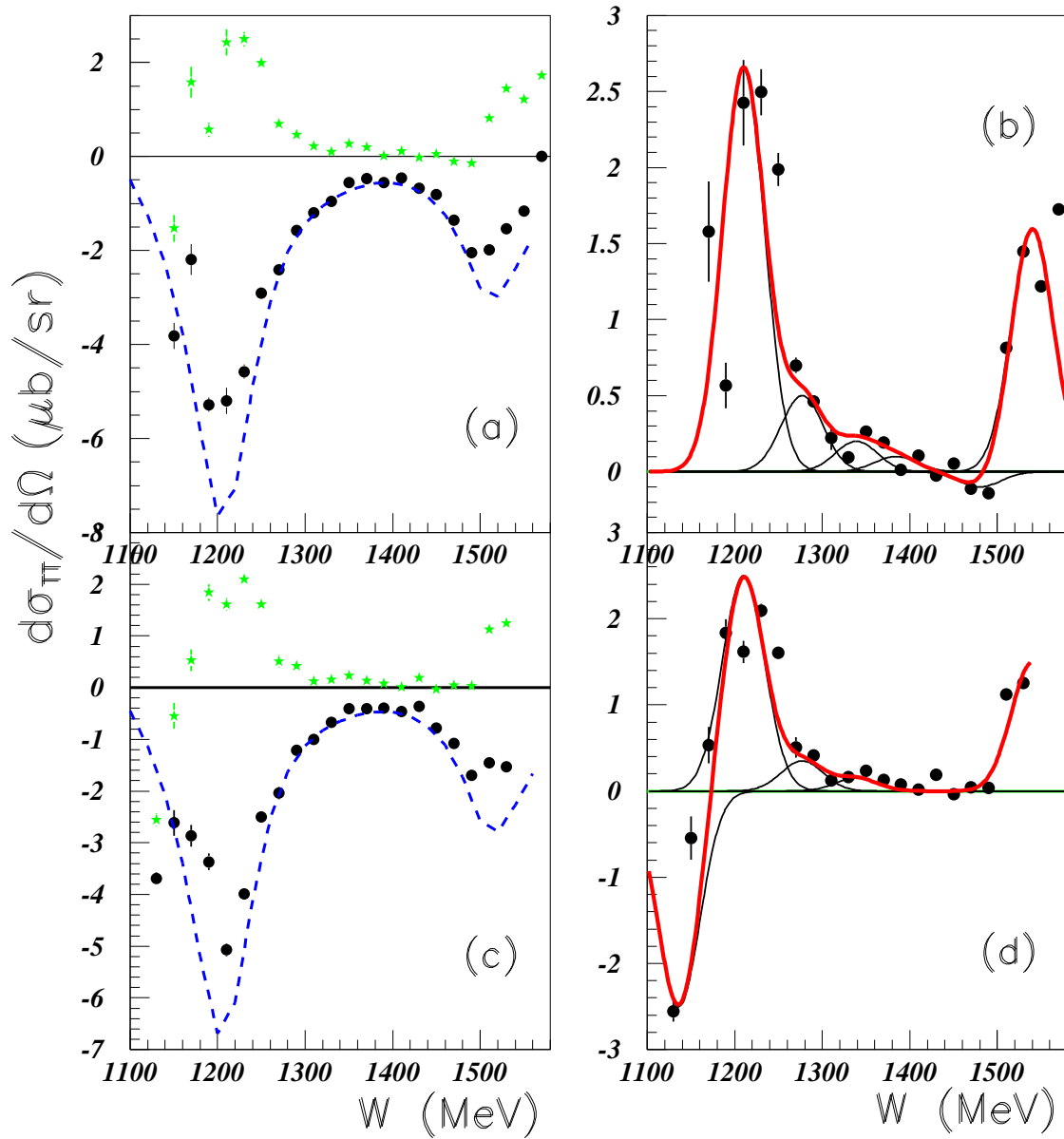


FIG. 27: Same as in Fig. 21, but for $\theta=127.5^\circ$

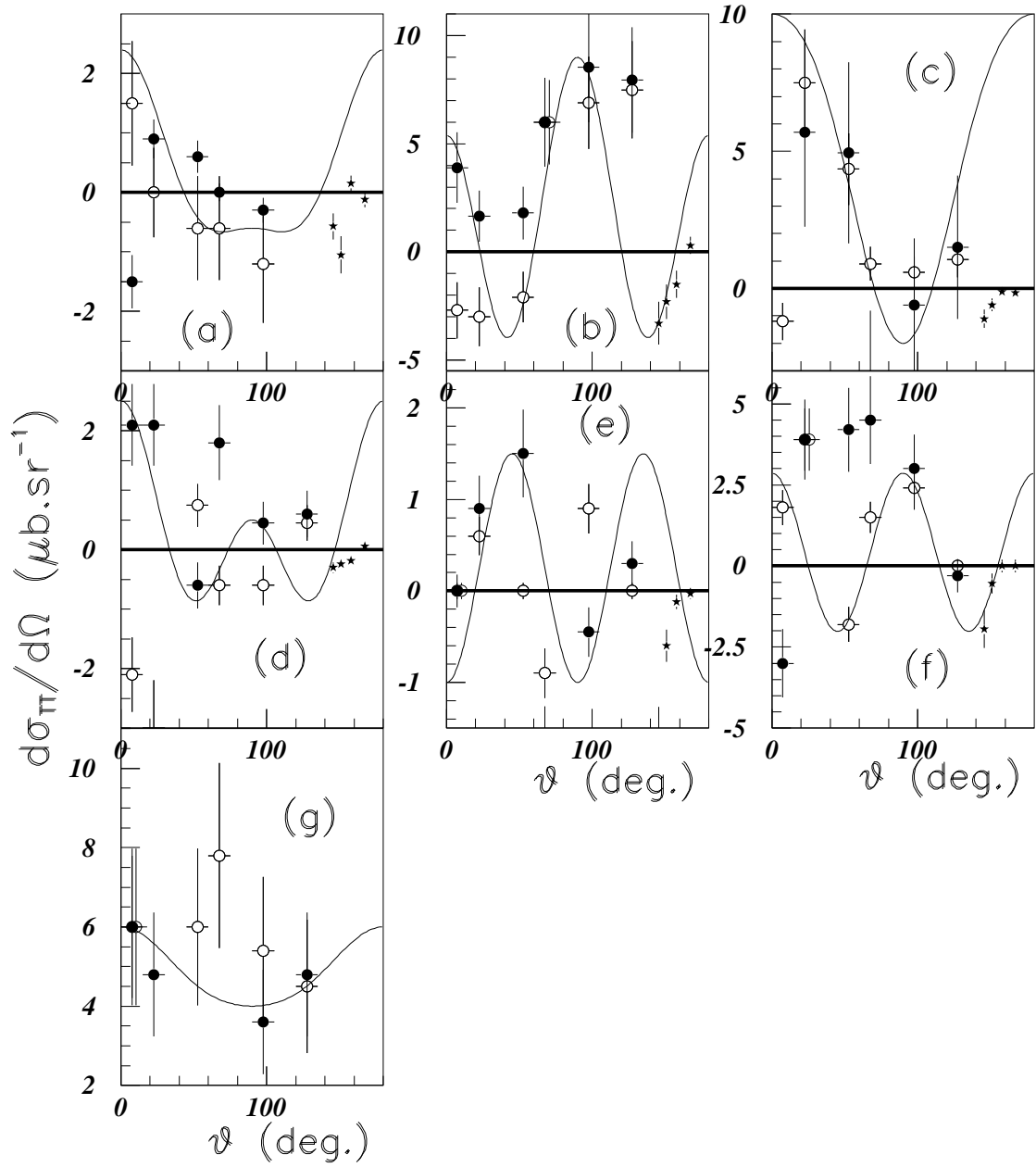


FIG. 28: Same as in Fig. 20 but showing the angular variation of the yield of the σ_{TT} structure function for both reactions.

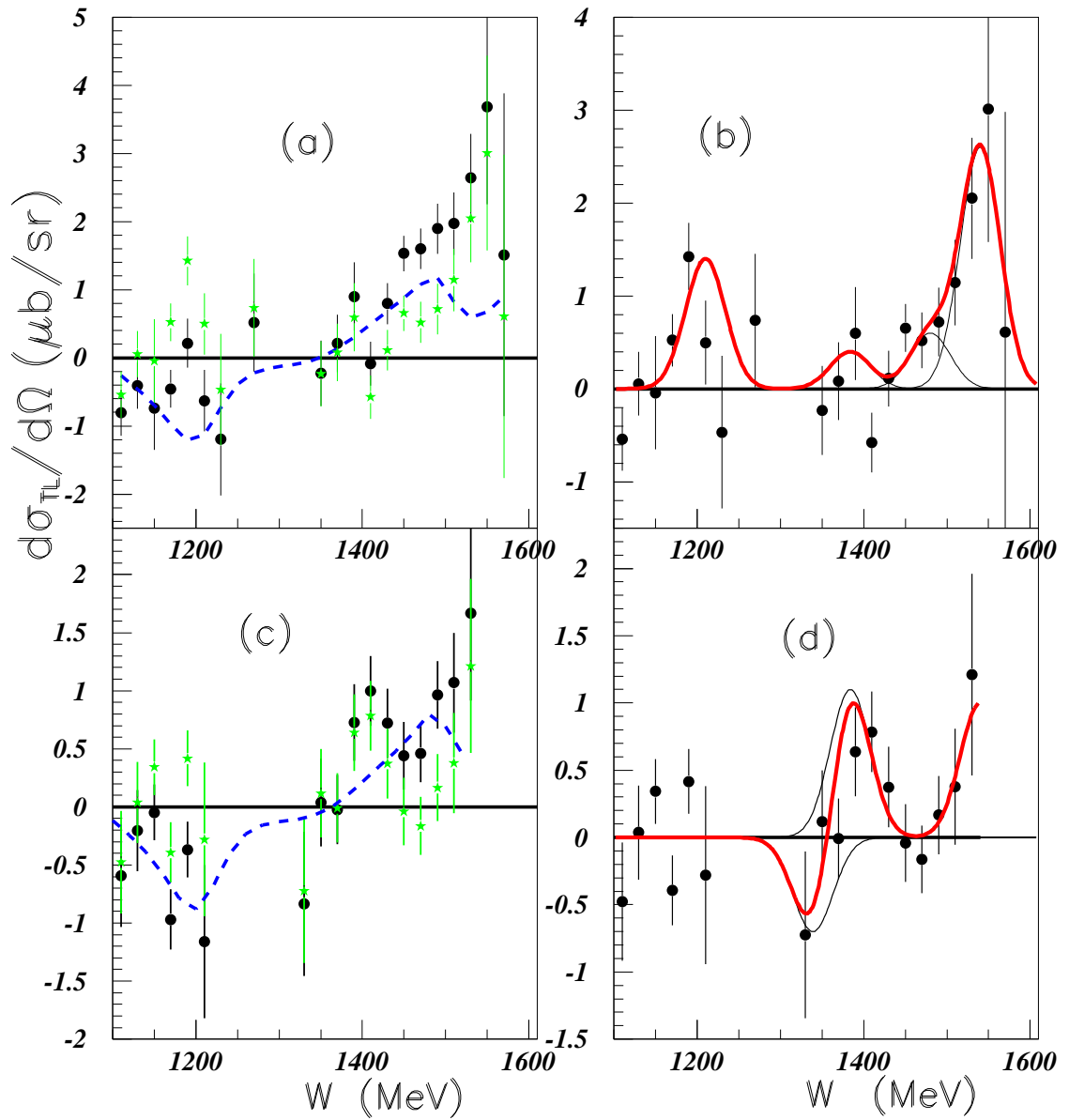


FIG. 29: Cross-section of the σ_{TL} structure function of the $ep \rightarrow e'n\pi^+$ reaction at $\theta=7.5^\circ$. Inserts (a) and (b) show the results at $Q^2=0.3 \text{ GeV}^2$, inserts (c) and (d) show the results at $Q^2=0.4 \text{ GeV}^2$.

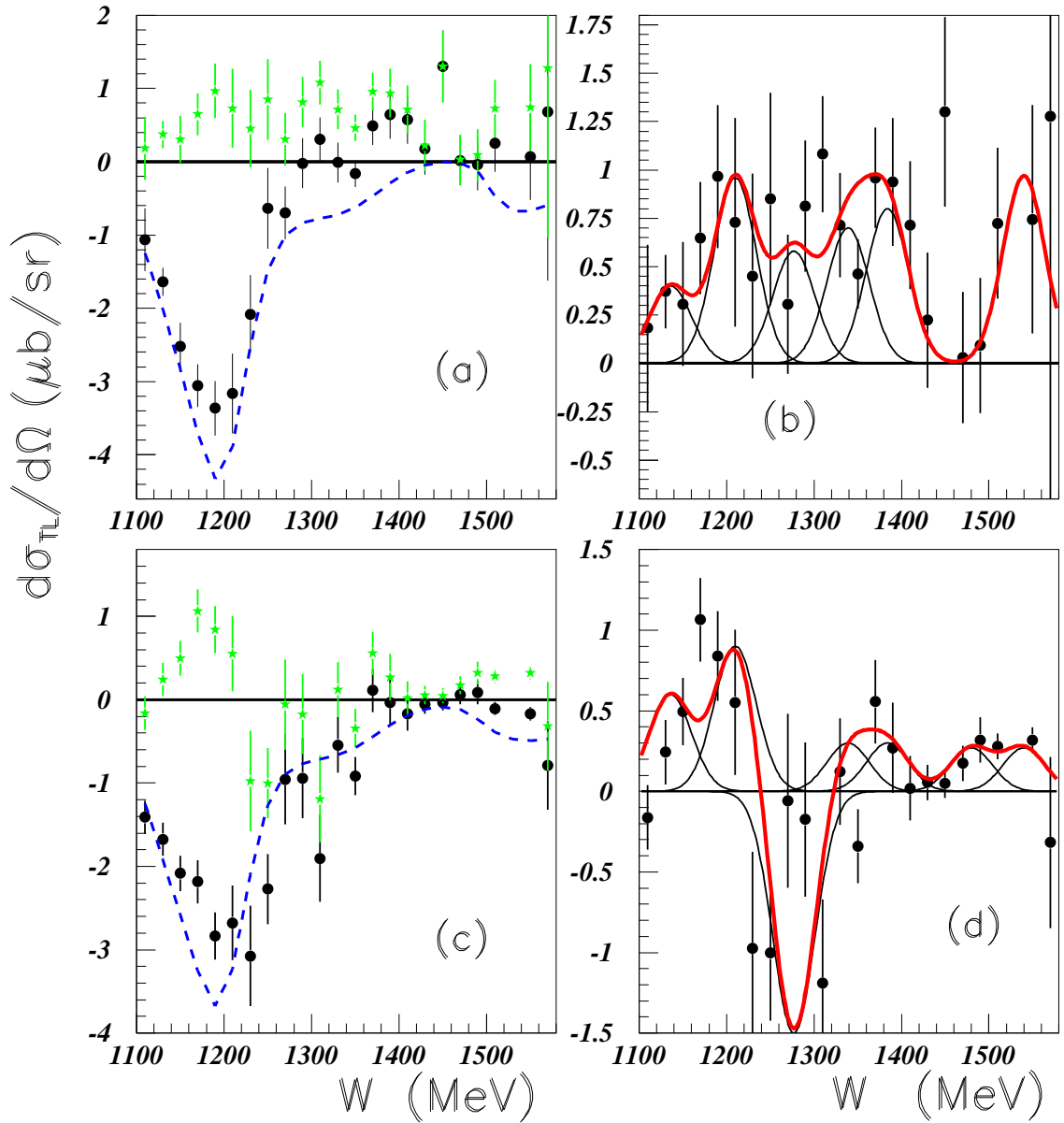


FIG. 30: Cross-section of the σ_{TL} structure function of the $ep \rightarrow e'n\pi^+$ reaction at $Q^2 = 0.3 \text{ GeV}^2$. Inserts (a) and (b) show the results for $\theta = 52.5^\circ$, inserts (c) and (d) show the results for $\theta = 67.5^\circ$.

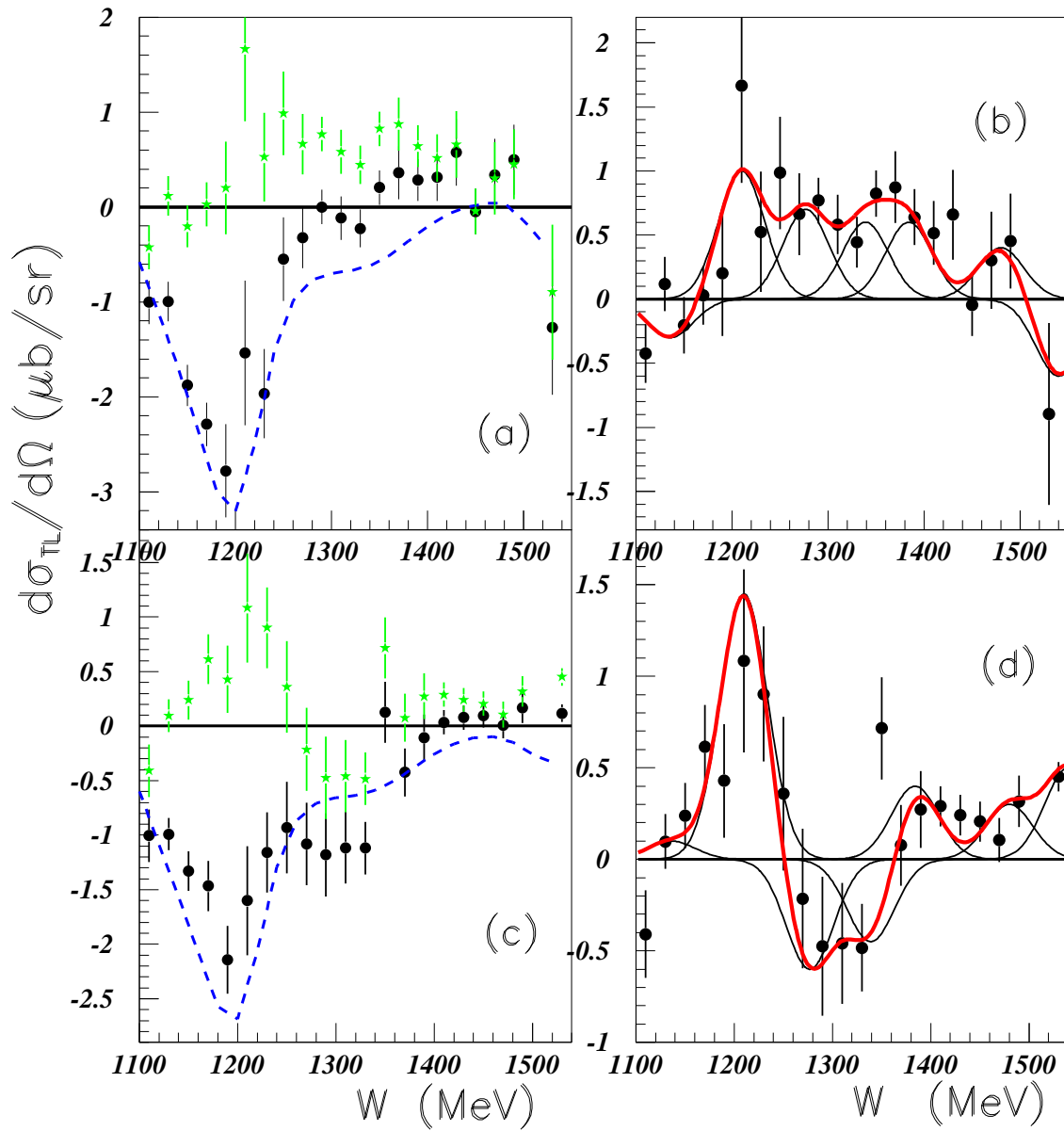


FIG. 31: Same as in Fig. 30, but for $Q^2=0.4 \text{ GeV}^2$.

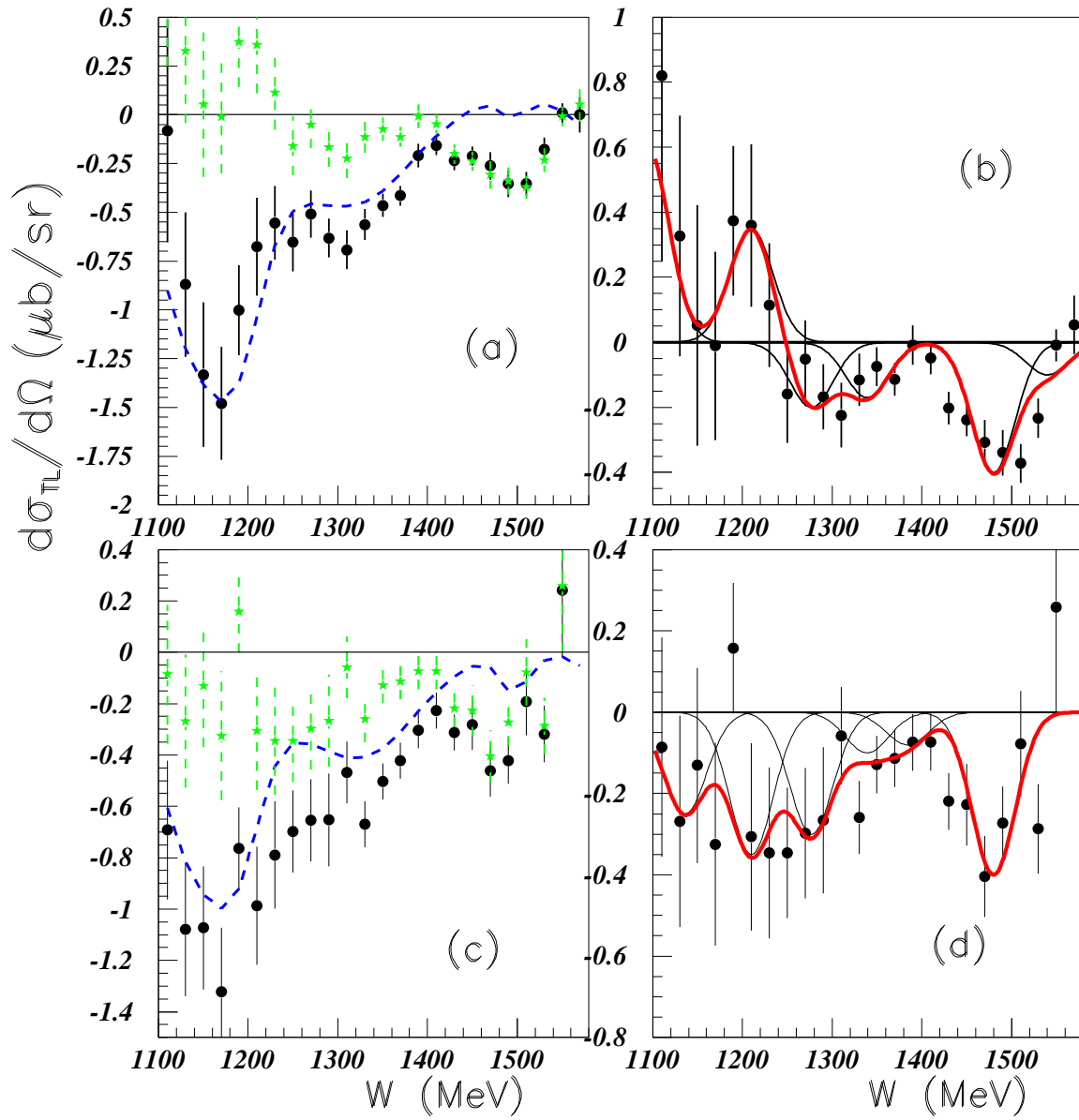


FIG. 32: Same as in Fig. 29, but for $\theta=97.5^\circ$.

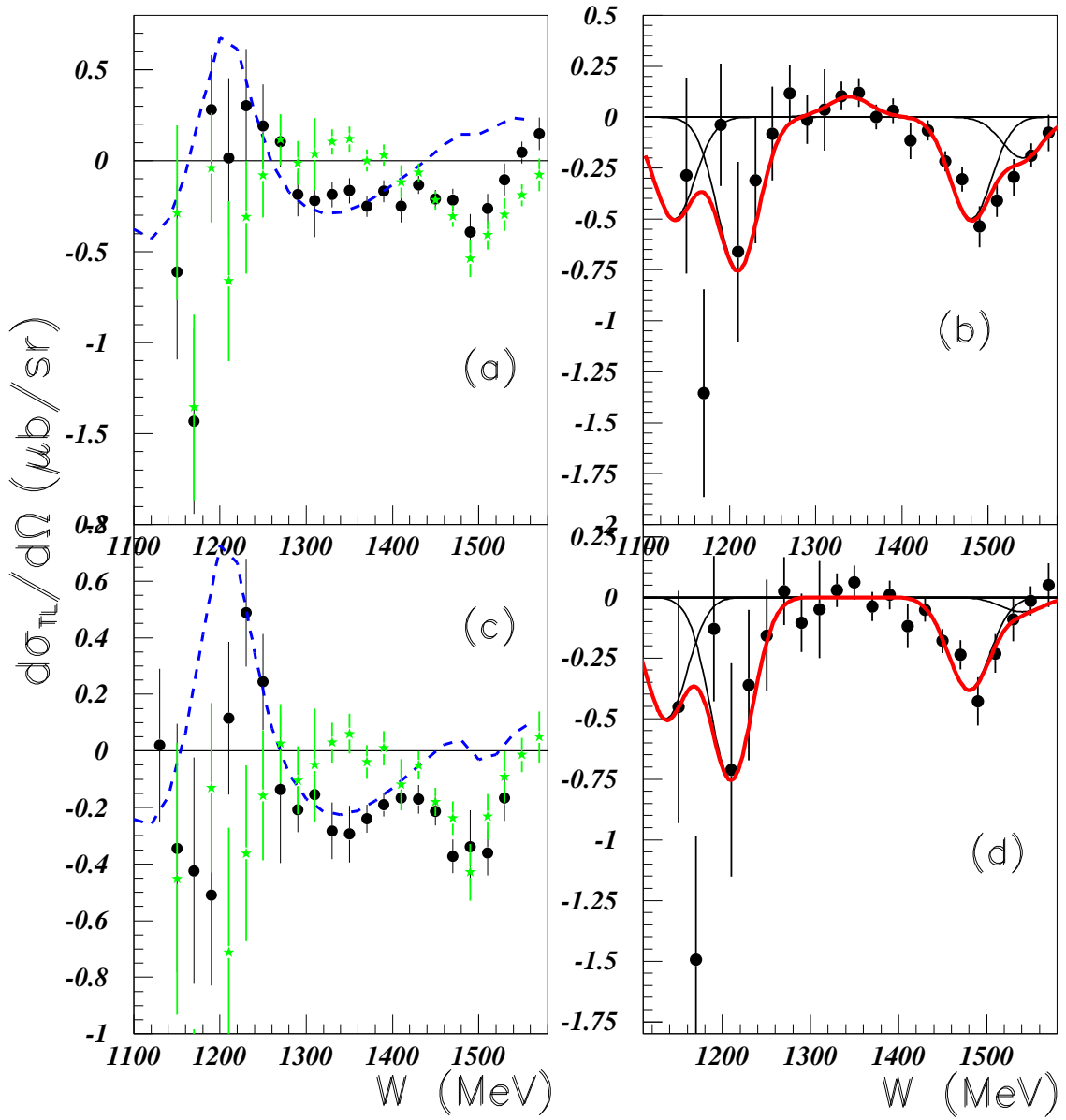


FIG. 33: Same as in Fig. 29, but for $\theta=127.5^\circ$.

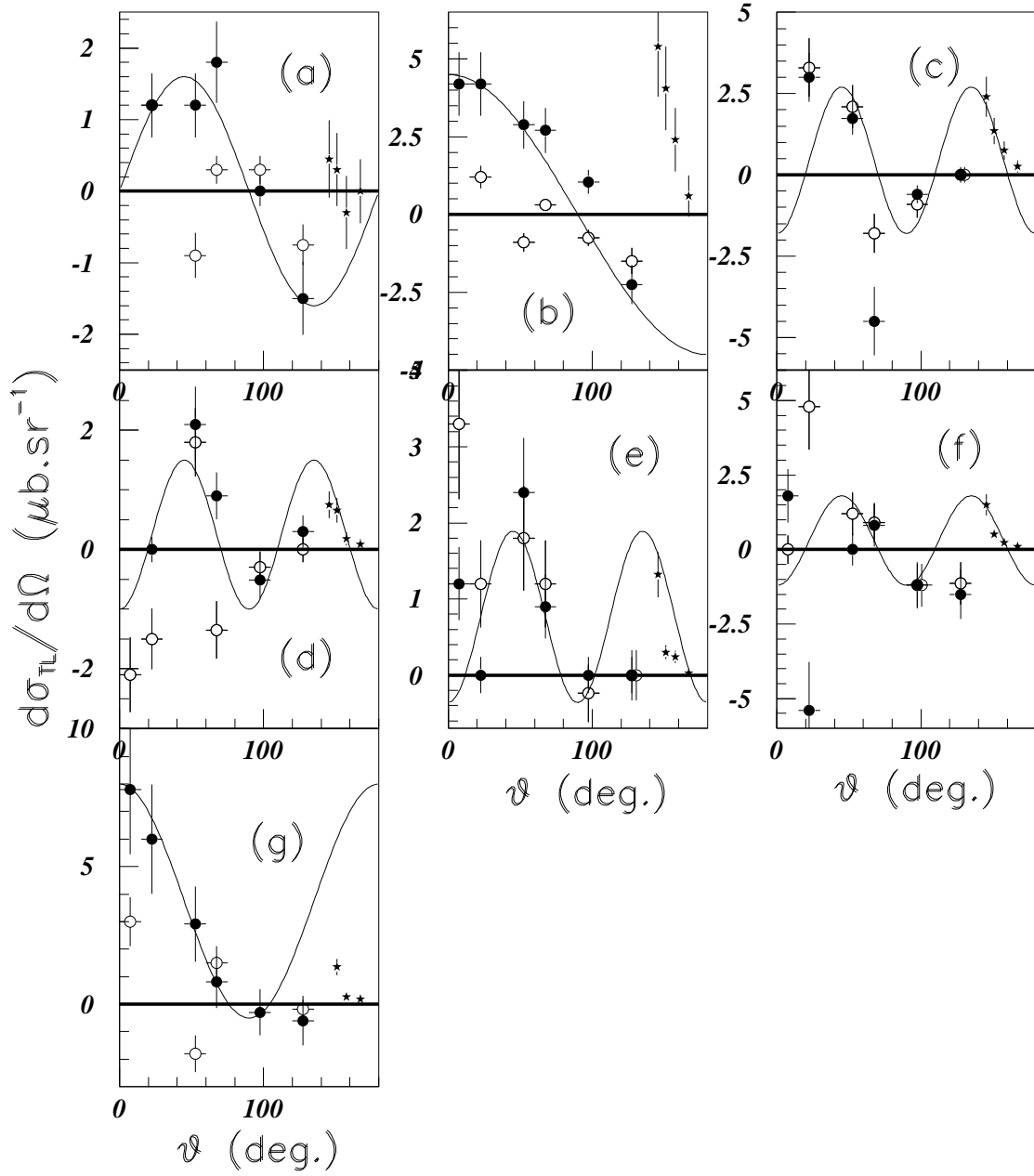


FIG. 34: Same as in Fig. 20 but showing the angular variation of the cross-sections corresponding to the σ_{TL} structure function for both reactions.

TABLE I: Masses (in MeV) of narrow exotic baryons, observed previously in SPES3 data and extracted from previous $p(\alpha, \alpha')X$ spectra measured at SPES4 [11] [12].

SPES3 mass	1004	1044	1094	1136	1173	1249	1277	1339	1384		1479	
pic marker	(a)	(b)	(c)	(d)	(e)	(f)	(g)	(h)	(i)	(j)	(k)	(l)
SPES4 mass 0.8^0		1052	1113	1142	1202	1234	1259		1370	1394		1478
SPES4 mass 2^0	996	1036	1104	1144	1198	1234		1313	1370			1477
SPES3 mass	1505	1517	1533	1542	(1554)	1564	1577					
pic marker	(m)	(n)	(o)	(p)	(q)	(r)	(s)					
SPES4 mass 2^0	1507	1517	1530	1544	1557	1569	1580					

TABLE II: Tentative attribution of isospin, using figs. 20, 28, and 34, for the narrow structures (see text). Inserts (a), (b), (c), (d), (e), (f), and (g) correspond respectively to the following masses: M=1136 MeV, 1210 MeV, 1277 MeV, 1339 MeV, 1384 MeV, 1480 MeV, and 1540 MeV.

insert	(a)	(b)	(c)	(d)	(e)	(f)	(g)
$\sigma_T + \epsilon\sigma_L$	1/2	3/2	3/2	1/2	1/2	1/2	3/2
σ_{TT}	1/2	3/2	1/2	1/2	1/2	3/2	1/2
σ_{TL}	1/2	1/2	3/2	3/2	3/2	3/2	1/2